remote sensing

MDPI

Article

Time-Efficient Multi-Region SAR Imaging with Heterogeneous UAVs: Joint Task Assignment and Path Planning

Deyu Song [1,2], Xiangyin Zhang [1,2,3,*], Baichuan Wang [1,2], Yalin Zhong [1,2], Yuan Yao [1] and Kaiyu Qin [1,2,3]

[1] School of Aeronautics and Astronautics, University of Electronic Science and Technology of China, Chengdu 611731, China; dysong@std.uestc.edu.cn (D.S.); bcwang@std.uestc.edu.cn (B.W.); 202422100121@std.uestc.edu.cn (Y.Z.); 202312100630@std.uestc.edu.cn (Y.Y.); kyqin@uestc.edu.cn (K.Q.)
[2] Aircraft Swarm Intelligent Sensing and Cooperative Control Key Laboratory of Sichuan Province, Chengdu 611731, China
[3] National Laboratory on Adaptive Optics, Chengdu 610209, China
* Correspondence: zhangzxy@uestc.edu.cn

Highlights

What are the main findings?

- A joint optimization framework is developed for heterogeneous SAR-UAV task assignment and path planning in multi-region imaging missions.
- The proposed ADCP and DSBOA methods improve workload matching and path quality, reducing mission completion time compared with baseline methods.

What is the implication of the main findings?

- The proposed framework provides a practical solution for improving SAR information acquisition efficiency in realistic multi-region imaging applications.

Abstract

Unmanned aerial vehicles (UAVs) provide a highly flexible platform for synthetic aperture radar (SAR), enabling efficient, high-quality imaging in remote sensing applications. In realistic imaging missions, regions of interest (ROIs) usually have different sizes and spatial distributions. While deploying SAR-UAVs with heterogeneous flight and imaging capabilities can improve mission time efficiency, realizing this improvement depends critically on task assignment and path planning. In this paper, the joint task assignment and path planning problem for heterogeneous SAR-UAVs in multi-region imaging missions is addressed. First, flight and imaging models of SAR-UAVs are established, and a constrained optimization problem is formulated to minimize the mission completion time. Then, an improved clustering strategy based on area-density and cost prediction (ADCP) is proposed to align ROI-dependent imaging workloads with heterogeneous SAR-UAV capabilities, thereby leveraging capability advantages and reducing the mission completion time. Finally, a discrete secretary bird optimization algorithm (DSBOA) is developed to generate feasible, high-quality paths. To accelerate convergence, UAV paths are encoded as waypoint sequences, and a mutation-based operator is introduced to update the population. Extensive Monte Carlo simulations show that the proposed approach consistently outperforms the baselines in mission completion time, demonstrating its effectiveness in improving time efficiency for multi-region SAR imaging missions. Ablation experiments further confirm the independent contributions of the proposed ADCP method and DSBOA algorithm.

Keywords: synthetic aperture radar (SAR); heterogeneous UAVs; task assignment; path planning

Check for updates

Academic Editor: Ming-Der Yang

Received: 18 March 2026
Revised: 27 April 2026
Accepted: 11 May 2026
Published: 13 May 2026

Copyright: © 2026 by the authors. Licensee MDPI, Basel, Switzerland. This article is an open access article distributed under the terms and conditions of the Creative Commons Attribution (CC BY) license.

1. Introduction

Due to high mobility, low operational cost, and strong adaptability [1], unmanned aerial vehicles (UAVs) have emerged as a key technology in remote sensing applications [2–4]. Equipped with synthetic aperture radar (SAR), UAVs can provide all-day, all-weather, high-resolution imaging of designated regions, enabling reliable sensing capabilities in complex and dynamic environments.

In realistic SAR imaging tasks, regions of interest (ROIs) typically have different sizes and spatial distributions. Under diverse regional workloads, a homogeneous UAV swarm with identical sensing and flight capabilities may suffer from limited mission flexibility and inefficient resource utilization [5]. To address this limitation, increasing research and practical efforts have focused on deploying UAVs with diverse flight capabilities and onboard sensing performance [6,7]. By leveraging complementary characteristics, heterogeneous UAVs can collaboratively satisfy diverse regional sensing requirements through balanced workload allocation, thereby improving time efficiency. For instance, long-endurance UAVs can rapidly image large regions, while high-resolution UAVs perform precise imaging over critical small regions. However, such advantages critically depend on jointly optimizing task assignment and path planning, which becomes substantially more challenging when deploying heterogeneous UAVs [8].

As illustrated in Figure 1, the studied problem is defined by two tightly coupled sub-problems: assigning regions to SAR-UAVs and planning feasible paths for each SAR-UAV. To obtain a feasible, high-quality solution, heterogeneous UAV capabilities, diverse region characteristics, and various mission constraints must be comprehensively considered. As a result, the joint task assignment and path planning problem is fundamentally NP-hard, involving combinatorial optimization under stringent constraints [9]. Moreover, its computational complexity grows rapidly with the number of target regions and UAVs, while the coexistence of UAV heterogeneity and region-dependent imaging workload further enlarges the decision space and strengthens variable coupling, making solution strategies designed for homogeneous UAV swarms inefficient.

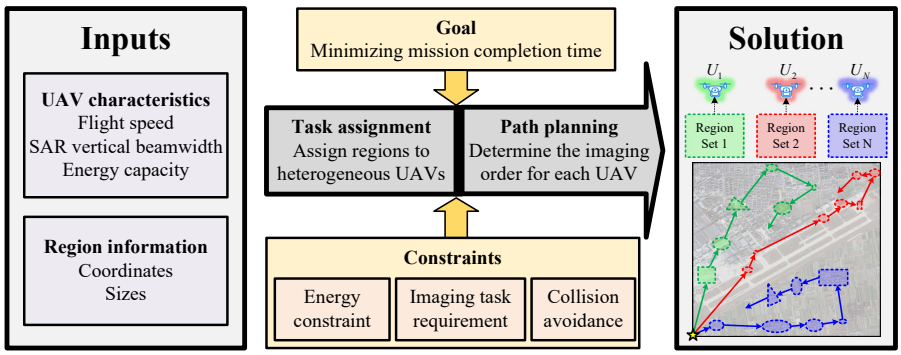


Figure 1. Problem definition of joint task assignment and path planning for heterogeneous SAR-UAVs. The star denotes the base station.

Addressing the above challenges has attracted increasing research interest [10]. However, most existing methods neglect region-specific imaging workloads, focusing solely on spatial distribution. Furthermore, current approaches fail to explicitly align heterogeneous regional imaging workloads with UAV-specific capabilities during task assignment [11], leading to inefficient allocations and degraded time efficiency. Additionally, path planning for individual UAVs assigned numerous regions is computationally intensive and often converges slowly.

Motivated by the above gaps, the joint task assignment and path planning problem for heterogeneous SAR-UAV imaging multiple target regions is addressed in this paper. A dual-stage methodology that integrates an improved area-density-based clustering strategy for

task assignment with a discrete metaheuristic path planner is developed. Near-optimal flight paths for SAR-UAVs are generated to image all target regions while minimizing the mission completion time subject to multiple constraints. The main contributions are summarized as follows:

- The joint task assignment and path planning model for heterogeneous SAR-UAVs covering multiple target regions is formulated. The UAV flight model, SAR imaging model, joint optimization objective, and multiple constraints are analyzed. Mission completion time is minimized by jointly considering heterogeneous flight and SAR imaging capabilities of SAR-UAVs and diverse region-dependent imaging workloads, a combination that has rarely been addressed in existing studies.
- An improved clustering strategy based on area density and cost prediction (ADCP) is developed for task assignment. An area-density-aware cluster center selection scheme and a KNN-based flight-workload metric for UAV–cluster assignment are introduced. Heterogeneous UAV flight capabilities are tightly aligned with region areas and spatial distributions during task assignment, which is insufficiently addressed in the existing literature.
- In the region clustering phase of ADCP, an edge-region-prioritized grouping strategy is adopted to prevent regions from being grouped into distant clusters. Solution feasibility is ensured by screening candidate SAR-UAVs based on predicted energy consumption, while solution quality is improved by selecting assignments that minimize the predicted mission completion time. A distance-based clustering mechanism is adaptively triggered to enhance robustness under UAV-scarce conditions.
- A discrete secretary bird optimization algorithm (DSBOA) is developed to generate a path for each SAR-UAV. A mutation-based sequence operator is introduced to replace the continuous population updates, thereby accelerating convergence. Near-optimal feasible paths for all SAR-UAVs can be generated.

The rest of this paper is organized as follows. Section 2 reviews related work. Section 3 establishes a precise formulation for the joint task assignment and path planning problem, specifying system constraints and the optimization objective. Section 4 details the proposed methodology, integrating the improved clustering strategy ADCP for task assignment with the DSBOA for path planning. Section 5 analyses the computational complexity of the proposed method. Section 6 presents comprehensive experimental results through rigorous benchmarking against representative methods. Concluding remarks are provided in Section 7.

2. Related Works

In general, existing studies on UAV task assignment and path planning can be broadly categorized into offline and online paradigms [12]. Online approaches update UAV decisions in real time during mission execution to cope with unforeseen changes. In recent online planning studies, deep reinforcement learning (DRL) [13,14] and multi-agent deep reinforcement learning (MADRL) [15] have been widely investigated for dynamic UAV decision-making problems. However, these methods usually require a pre-trained policy under scenario-specific state-space, action-space, and reward-function designs. For emergency sensing missions, the training scenarios may not accurately match the current mission requirements, which may degrade policy generalization and lead to suboptimal mission performance. Training a new policy for each emergency mission would also introduce substantial additional time and computational cost, weakening the timeliness required by pre-mission planning. This work focuses on offline joint task assignment and path planning for multi-region SAR imaging missions. In this setting, mission information is available before execution, and the problem can be directly solved as a static combinatorial

optimization problem without policy pre-training or task-specific training datasets. Therefore, offline combinatorial optimization methods are suitable for time-sensitive sensing scenarios. Accordingly, related offline UAV task assignment and path planning studies for SAR imaging missions are reviewed as follows.

Most existing studies on SAR-UAV imaging focus on individual targets or a single region, with primary objectives such as achieving high-quality imaging [16], enhancing communication-related performance [17], or improving power efficiency [18]. However, SAR information acquisition efficiency in multi-region missions has received limited attention. In existing studies that explicitly optimize time efficiency, the imaging mission is commonly formulated as a coverage problem [19], where the mission workload is approximated using only inter-region distances [20,21]. In realistic remote-sensing missions, SAR-UAVs are often required to image multiple separated ROIs. As the mission scale grows, the mission workload is determined not only by inter-region flight but also by the intra-region SAR imaging process, while the region-dependent imaging workload is usually neglected. Moreover, variations in ROI sizes can substantially influence the required SAR imaging time and thus the overall mission time efficiency, yet this factor is seldom explicitly considered in existing multi-region SAR imaging studies.

In heterogeneous SAR-UAV multi-region imaging missions, the time-efficiency challenge is closely related to the coupling between task assignment and path planning [22]. Task assignment determines how ROIs are allocated to individual UAVs, which in turn constrains the subsequent visiting sequence and spatial traversal range in path planning. Conversely, the flight distance and energy consumption induced by the planned paths affect whether the workload allocation remains feasible and efficient. Therefore, these two components should be jointly considered, leading to the joint task assignment and path planning problem. Extensive studies have investigated this problem in heterogeneous multi-UAV coverage missions using a two-stage solution architecture [20,23]. For example, the authors in [24] propose a spatial–temporal clustering-based algorithm for task assignment and introduce genetic algorithm to obtain approximate paths for heterogeneous UAV coverage. Although these studies demonstrate the feasibility of coordinating task assignment and path planning within an integrated framework, most of them still rely on simplified workload representations, where mission cost is mainly characterized by spatial traversal or coverage distance. As a result, the ROI-size-induced intra-region coverage workload is not explicitly modeled, which restricts the quality of workload balancing and the mission-time efficiency in heterogeneous multi-UAV coverage missions.

Despite the above efforts on joint optimization, many existing studies still investigate task assignment and path planning separately in multi-region heterogeneous UAV coverage missions.

In the broader literature on heterogeneous UAV task assignment, the problem is often formulated as a mixed integer linear programming (MILP) model with complex constraints. Traditional integer programming methods are often computationally prohibitive for practical applications due to the NP-hard complexity of MILP problems [25]. Metaheuristic-based methods have gained prominence for efficiently obtaining near-optimal solutions within a practical number of iterations. Approaches such as particle swarm optimization [8], ant colony optimization [26], fruit fly optimization [27], and symbiotic organisms search [28] have been widely applied to UAV task assignment. These methods share an iterative search mechanism in which populations of candidate solutions are gradually refined to approximate a global optimum. Clustering-based methods have also attracted increasing research attention in UAV swarm task assignment due to their favorable computational efficiency. Clustering methods such as fuzzy C-means [29], K-means [30], and density peak clustering [31] demonstrate comparable solution quality to metaheuristics with sig-

nificantly reduced computational cost in task assignment problems. To further enhance clustering-based assignment for heterogeneous UAVs, Chen et al. [8] propose an adaptive clustering-based algorithm to allocate a bounded number of regions to heterogeneous UAVs. Despite these different solution paradigms, the explicit matching between region-dependent coverage workload and heterogeneous UAV capabilities remains insufficiently addressed in existing methods. This limitation becomes particularly pronounced in heterogeneous SAR-UAV multi-region imaging missions, where ROI size directly affects the required imaging workload.

Path planning for UAVs has been extensively studied. Such problems are commonly formulated as MTSP or VRP coverage planning problems, where each UAV must determine the visiting order of its assigned regions. In typical coverage and surveillance missions, UAVs are set to operate at a prescribed sensing altitude to satisfy safety and sensing requirements [32]. Under this setting, the 3D trajectory can be reasonably projected onto a planar map. The 2D formulation reduces modeling and computational complexity without sacrificing the fidelity required for region-coverage scheduling. Existing offline path planning methodologies are broadly categorized into two approaches: geometric-based and metaheuristic-based. Geometric-based approaches, such as A* [33] and Dijkstra's algorithm [34], usually rely on repeated graph search or heuristic node expansion to generate feasible paths, but their scalability may deteriorate in large-scale coverage scenarios. Metaheuristic-based methods have therefore attracted increasing attention in heterogeneous UAV path planning [35]. Improved variants of metaheuristics, such as the multi-objective evolutionary algorithm in [36], the hybrid golden jackal–moth flame optimization algorithm in [37], and the ant colony system-based method in [7], are mainly designed to improve convergence behavior and can efficiently generate feasible coverage paths in heterogeneous UAV missions. Nevertheless, path planning essentially remains a combinatorial visiting-sequence optimization problem, whose search space is high-dimensional and highly complex. As a result, rapid convergence is still difficult to achieve, and the solution efficiency of existing heterogeneous UAV path planning methods requires further improvement.

Overall, despite substantial research on heterogeneous UAV coverage, task assignment, path planning, and their joint optimization, several critical limitations remain for heterogeneous SAR-UAV multi-region imaging missions. First, most existing formulations still approximate mission workload through inter-region distances, while the ROI-size-induced intra-region SAR imaging workload is rarely modeled explicitly. As a result, the actual imaging time cost is underestimated, leading to inefficient workload allocation. Second, current task assignment methods do not adequately capture the explicit matching between region-dependent workload and heterogeneous UAV flight and imaging capabilities, which may result in mismatched assignments and degraded mission time efficiency. Third, existing path planning methods still suffer from slow convergence and a susceptibility to local optima, particularly in large-scale multi-region missions where the solution space remains high-dimensional and highly complex. Therefore, further study of the joint task assignment and path planning problem for heterogeneous SAR-UAV multi-region imaging remains necessary for improving SAR information acquisition efficiency.

3. Model Establishment and Problem Formulation

3.1. System Model

Consider N UAVs $\{U_1, U_2, \cdots, U_N\}$ equipped with SAR sensors deployed to image M target regions $\{R_1, R_2, \cdots, R_M\}$ distributed in a designated mission area. In practical missions, target regions are usually of different sizes, given by $\{S_1, S_2, \ldots, S_M\}$. The path planning results are represented by $Q = \{Q_i | i \in [1, N]\}$, where each element Q_i defines

the flight path for U_i. Regions and the base are labeled with unique identifiers: the regions are denoted by 1 to M, and the base is labeled as 0. Each path Q_i consists of an ordered sequence of region identifiers, defining the imaging sequence for U_i. The first and last elements of Q_i are always 0, ensuring all SAR-UAVs depart from the base, sequentially image their assigned regions, and finally return to the base.

A distance matrix $D = \left\{ D_{j,k} | j,k \in [0,M] \right\}$ is used to store the Euclidean distances between regions, where $D_{j,k}$ represents the flight distance between regions R_j and R_k. Specifically, $D_{0,j} = D_{j,0}$ denotes the Euclidean distance between the base R_0 and region R_j. All distances can be calculated from the coordinates of the target regions and the base.

In this study, the side-looking stripmap SAR mode is adopted, as it provides continuous ground coverage along the flight direction and is well suited for regional imaging tasks. To enhance mission flexibility under varying imaging requirements, the UAVs are assumed to have diverse flight speeds and onboard SAR vertical beamwidths. Accordingly, each UAV is characterized by $U_i = \{V_i, \theta_i\}$, where V_i and θ_i denote its flight speed and SAR vertical beamwidth, respectively. The flight altitude H and look angle α of the SAR-UAVs are selected to satisfy the required imaging quality and are assumed identical during mission execution to maintain consistent imaging geometry for stable stripmap imaging performance. Under these assumptions, all flight paths are projected onto a 2D planar map for high-level task assignment and path planning.

This study considers an offline pre-mission planning setting for static multi-region SAR imaging tasks, where the ROI locations, region sizes, base station position, and UAV capability parameters are known a priori. The formulation is primarily intended for open environments in remote-sensing missions where imaging is the primary task. Under such conditions, mission completion time is mainly determined by inter-region transit and intra-region SAR imaging workload. The formulation focuses on the high-level task assignment and inter-region path planning layer, rather than detailed low-level flight control, obstacle-constrained trajectory generation, or communication-aware coordination.

The UAV flight model, side-looking SAR imaging model, and exact problem formulation are presented as follows.

3.1.1. UAV Flight Model

In practical large-scale area imaging tasks, UAVs commonly operate at a steady flight speed to simplify energy management and to maintain stable imaging performance. Accordingly, in this work, each SAR-UAV is assumed to fly with a constant horizontal velocity during mission execution. Such an assumption enables a tractable formulation of the mission completion time and propulsion energy consumption.

For a given flight path Q_i of U_i, the total flight distance is denoted as D_{Q_i}, and the associated flight time of U_i can be calculated as

$$T_{\text{Fly}}^{i} = \frac{D_{Q_i}}{V_i}. \tag{1}$$

The onboard energy consumption of a rotor UAV mainly comprises imaging energy and propulsion energy. Since the imaging energy is typically negligible compared with the propulsion energy, it is not considered in this study. According to [38], the propulsion power of U_i can be expressed as:

$$P_i = P_0 \left(1 + \frac{3V_i^2}{U_{\text{tip}}^2} \right) + P_1 \left(\sqrt{1 + \frac{V_i^4}{4v_0^4}} - \frac{V_i^2}{2v_0^2} \right)^{1/2} + \frac{1}{2} d_0 \rho S_0 A_0 V_i^3, \tag{2}$$

where P_0 denotes the blade profile power, and P_1 is the induced power in the hovering state. U_{tip} denotes the tip speed of the rotor blade, and v_0 denotes the average rotor induced velocity in hover. d_0, ρ, S_0, and A_0 are UAV-related aerodynamic parameters.

3.1.2. Side-Looking SAR Imaging Model

As shown in Figure 2a, each SAR-UAV maintains a fixed look angle α and flies at altitude H under the side-looking stripmap SAR mode. The ground-range swath width of U_i can be calculated as

$$W_i = H\left[\tan\left(\alpha + \frac{\theta_i}{2}\right) - \tan\left(\alpha - \frac{\theta_i}{2}\right)\right]. \tag{3}$$

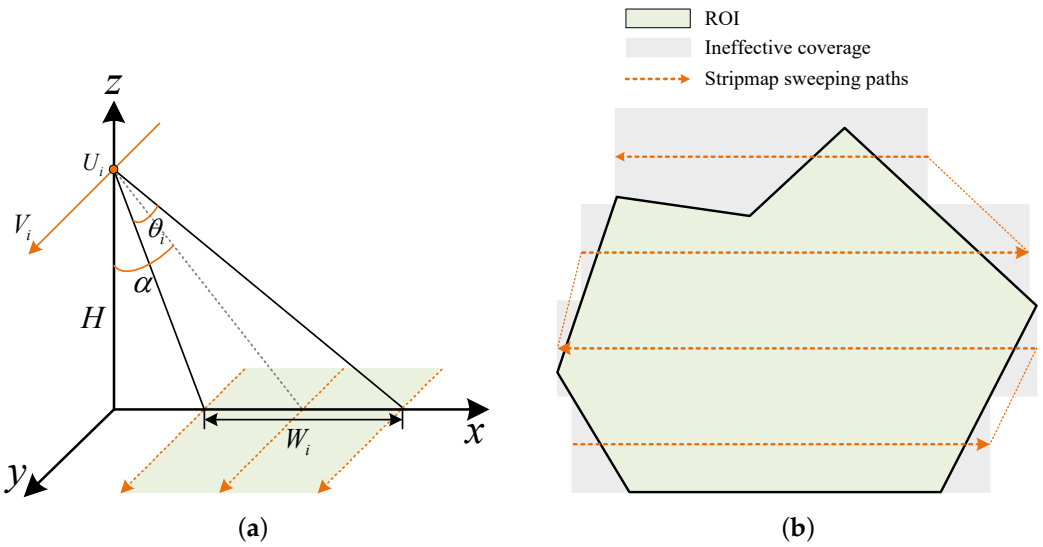


Figure 2. Illustrations of the SAR imaging model: (**a**) imaging geometry of side-looking SAR; (**b**) predefined stripmap SAR sweeping pattern over an irregular ROI.

Therefore, the ground area imaged by U_i per unit time can be defined as

$$\Lambda_i = V_i \cdot W_i. \tag{4}$$

To focus on the joint task assignment and path planning problem, the detailed intra-region SAR scanning paths are not optimized in this work. Instead, as shown in Figure 2b, a predefined stripmap SAR sweeping pattern is adopted, in which the UAV flies along parallel adjacent paths to achieve full ground coverage, as commonly used in stripmap SAR-based imaging systems [39].

In practical missions, target regions usually have irregular polygonal shapes, which may lead to coverage inefficiency or local overlap near irregular boundaries under the adopted SAR sweeping pattern. Therefore, a coefficient $\kappa \in (0, 1]$ is introduced to describe the coverage efficiency degradation. For a target region R_j with area S_j, the intra-region SAR imaging time required by U_i can thus be modeled as

$$T_{\text{Img}}^{i,j} = \frac{S_j}{\kappa \cdot \Lambda_i} = \frac{S_j}{\kappa \cdot V_i \cdot W_i}. \tag{5}$$

3.2. Problem Formulation

This subsection presents an exact formulation of the joint task assignment and path planning problem for heterogeneous SAR-UAVs to image multiple regions.

To simplify the model and facilitate computation, this work focuses exclusively on the imaging capabilities, flight speeds, and energy constraints, while excluding considerations such as obstacle avoidance and communication. Therefore, for a given path Q_i, the UAV mission time cost can be calculated as

$$\begin{aligned} T(Q_i) &= T^i_{\text{Fly}} + \sum_{j \in \mathcal{J}(Q_i)} T^{i,j}_{\text{Img}} \\ &= \frac{D_{Q_i}}{V_i} + \sum_{j \in \mathcal{J}(Q_i)} \frac{S_j}{\kappa \cdot V_i \cdot W_i}, \end{aligned} \tag{6}$$

where $\mathcal{J}(Q_i)$ denotes the set of target regions assigned to U_i (excluding the base).

The mission completion time is defined as the maximum mission time cost across all UAVs, which can be calculated via

$$T(Q) = \max_{1 \le i \le N} T(Q_i). \tag{7}$$

To ensure mission feasibility under practical operational limitations, the following constraints must be satisfied.

(1) Energy capacity constraint: The energy consumed by U_i while executing along path Q_i must not exceed its maximum energy capacity $E^i_{\max}$. Since the propulsion power is consumed throughout both flight and imaging durations, the energy constraint can be expressed as:

$$\forall i \in [1, N], \quad P_i \cdot T(Q_i) \le E^i_{\max}. \tag{8}$$

(2) Imaging requirement constraint: To ensure task quality and avoid redundant resource allocation, each target region must be imaged by one and only one SAR-UAV. This constraint is formally defined as:

$$\begin{cases} \bigcup_{i=1}^{N} \mathcal{J}(Q_i) = \{1, 2, \ldots, M\}, \\ \mathcal{J}(Q_i) \cap \mathcal{J}(Q_k) = \emptyset, \quad \forall\, i, k \in [1, N],\ i < k. \end{cases} \tag{9}$$

(3) Overall task requirement constraint: All SAR-UAVs must start from and return to the base station R_0, which can be expressed via

$$\forall i \in [1, N], \quad Q_{i,1} = Q_{i,|Q_i|} = 0, \tag{10}$$

where $|Q_i|$ denotes the length of the ordered sequence in Q_i.

(4) Collision avoidance constraint: To guarantee safe operation, the inter-UAV separation distance should be no smaller than a predefined safety distance r_{safe} during mission execution. Let $\mathbf{q}_i(t) \in \mathbb{R}^2$ denote the sampled position of U_i at time t, which can be computed from Q_i together with the corresponding flight speeds. The collision avoidance constraint can thus be formulated as:

$$\forall\, i, k \in [1, N],\ i < k,\ \forall\, t \in [0, \min\{T(Q_i), T(Q_k)\}], \quad \|\mathbf{q}_i(t) - \mathbf{q}_k(t)\|_2 \ge r_{\text{safe}}. \tag{11}$$

Based on the objective and constraints defined above, the joint task assignment and path planning problem for multi-region imaging is stated as the following constrained minimization problem:

$$\begin{aligned} &\underset{Q}{\text{minimize}} \quad T(Q) \\ &s.t. \quad (8), (9), (10), (11). \end{aligned} \tag{12}$$

In the considered offline multi-region SAR imaging setting, mission completion time is selected as the optimization objective because it directly reflects mission-level SAR information acquisition efficiency in the studied high-level task assignment and path planning problem. Therefore, the present study adopts a single-objective design centered on mission completion time.

It should be noted that relaxing the assumptions of constant flight speed, identical flight altitude and look angle during imaging, and propulsion-dominant onboard energy consumption may improve physical realism and change the absolute mission-time or energy estimates, but would not be expected to substantially affect the relative performance under the present formulation. In addition, a more detailed intra-region imaging model may change the quantitative mission-time estimates and the magnitude of the observed performance improvements, but would not materially alter the qualitative comparative advantage of explicitly incorporating region-dependent imaging workload in the considered high-level task assignment and path planning problem.

4. Methodology

The formulated problem exhibits a natural two-stage structure. First, the ROIs are assigned to appropriate SAR-UAVs according to ROI characteristics and heterogeneous UAV capabilities. Then, the visiting order of the assigned ROIs is optimized for each SAR-UAV to further reduce the mission completion time. Specifically, an improved clustering strategy based on area density and cost prediction (ADCP) is developed for the task assignment stage. In this stage, heterogeneous UAV capabilities are explicitly handled by matching ROI clusters to UAV-specific flight and imaging characteristics. Subsequently, a discrete secretary bird optimization algorithm (DSBOA) is employed in the path planning stage to generate efficient visiting sequences for each SAR-UAV under this heterogeneous matching result. The main contributions of the proposed framework lie in redesigning the task assignment stage based on density peak clustering to incorporate ROI-dependent imaging workload and heterogeneous capability matching, and in adapting SBOA to a discrete visiting-sequence optimization framework for the considered path planning problem to further improve solution quality and convergence efficiency.

4.1. Improved Clustering Strategy Based on Area Density and Cost Prediction

The proposed ADCP clustering strategy has three phases. First, an area-density-aware cluster center selection phase is performed based on region sizes and spatial distribution characteristics. Subsequently, a UAV-center assignment phase strategically matches UAV flight capabilities to the spatial patterns of the selected cluster centers. Finally, regions are clustered according to energy constraints and predicted imaging mission times, with an adaptively triggered clustering strategy used to address flight-imaging workload imbalance.

4.1.1. Cluster Center Selection Phase

Density peak clustering (DPC) [40] has proven flexible and effective in UAV task assignment problems with large numbers of ROIs [41]. Its unique center-selection mechanism, based on local density and relative separation, is highly compatible with the task assignment requirement of identifying representative region centers for heterogeneous SAR-UAV allocation, especially under irregular ROI distributions. Accordingly, this work adapts the cluster center selection strategy from DPC. However, regions exhibit varied sizes in the considered problem. Consequently, relying solely on distance-based density fails to accurately characterize the expected imaging workload, which is defined as the cumulative area of regions required to be imaged within the vicinity of a cluster center.

Selecting centers based purely on distance density risks assigning excessive imaging area to individual clusters, thereby increasing mission completion time.

The proposed cluster center selection strategy quantifies the imaging workload ρ_j for region R_j as the sum of areas from neighboring regions within a cut-off distance:

$$\rho_j = \sum_{k=1,k\neq j}^{M} \chi(D_{j,k}) \cdot S_k, \tag{13}$$

where $D_{j,k}$ is the Euclidean distance between R_j and R_k. $\chi(\cdot)$ is the indicator function, which is defined as:

$$\chi(D_{j,k}) = \begin{cases} 1 & \text{if } D_{j,k} < d_c, \\ 0 & \text{otherwise,} \end{cases} \tag{14}$$

where d_c is determined from the pairwise-distance distribution of ROIs in the current task scenario. Let $\mathcal{D} = \{D_{j,k} \mid j,k \in [1,M], j \neq k\}$ denote the set of pairwise ROI distances, and let $d_{(1)} \leq d_{(2)} \leq \cdots \leq d_{(M(M-1))}$ be the sorted distances in ascending order. The cut-off distance is then selected as

$$d_c = d_{(\ell_c)}, \quad \ell_c = \max\{1, \text{round}(\eta_c M(M-1))\}, \tag{15}$$

where $\eta_c \in (0,1)$ is a preset percentile coefficient. This percentile-based rule allows d_c to adapt to the spatial scale and distribution of ROIs in each task scenario, while avoiding manual selection of an absolute cut-off distance for different cases.

The relative distance factor δ_j for R_j is defined as its minimum distance to any region with a higher imaging workload. For the region with the largest imaging workload $\rho_{\max}$, δ_j is its maximum distance to any other region. Thus, δ_j can be computed as:

$$\delta_j = \begin{cases} \min\limits_{k:\rho_k > \rho_j} D_{j,k} & \text{if } \rho_j < \rho_{\max}, \\ \max\limits_{k\in[1,M]} D_{j,k} & \text{otherwise.} \end{cases} \tag{16}$$

In the proposed clustering strategy, cluster centers should simultaneously exhibit high imaging workload and substantial isolation from regions with higher imaging workload. Therefore, a selection metric γ is defined based on the imaging workload ρ and relative distance factor δ to help select appropriate cluster centers:

$$\gamma_j = \rho_j \cdot \delta_j. \tag{17}$$

Eventually, the N regions with the largest γ values are selected as cluster centers. Each center will be assigned to a SAR-UAV during the subsequent cluster center assignment phase.

4.1.2. Cluster Center Assignment Phase

Following cluster center selection based on the imaging workload, a critical limitation emerges. Clustering without explicit UAV–cluster assignment may yield clusters whose imaging and flight workloads mismatch the heterogeneous capabilities of the SAR-UAVs. Specifically, clusters with heavy imaging workload might be assigned to SAR-UAVs with a narrow SAR swath width, or spatially dispersed clusters to SAR-UAVs with low flight speeds. Both situations potentially increase the mission completion time. To mitigate this limitation, each selected cluster center is immediately assigned to a specific SAR-UAV after the center selection phase, enabling subsequent clustering processes to explicitly incorporate UAV-specific flight and SAR imaging capabilities.

During the cluster center assignment phase, a K-nearest neighbor (KNN) [42] approach is introduced to quantify the expected flight workload for each cluster center. For a given cluster center R_j, its K-nearest neighbor set $\mathcal{N}_j$ is first constructed by identifying K closest regions. The average KNN nearest neighbor distance $\bar{D}^j_{\mathcal{N}}$ for center R_j is then computed as:

$$\bar{D}^j_{\mathcal{N}} = \frac{1}{K} \sum_{k \in \mathcal{N}_j} \min_{\substack{l \in [1,M] \\ l \neq k}} D_{k,l}, \tag{18}$$

where K is determined by the ratio of the number of regions to the number of SAR-UAVs:

$$K = \left\lfloor \frac{M}{N} \right\rfloor. \tag{19}$$

This setting makes the KNN neighborhood size consistent with the average number of ROIs expected to be assigned to each SAR-UAV.

The average KNN nearest neighbor distance captures the local spatial sparsity of the neighborhood associated with a cluster center. A larger value of $\bar{D}^j_{\mathcal{N}}$ indicates that the neighboring regions are more sparsely distributed, implying higher flight-speed demand for imaging the cluster. Consequently, $\bar{D}^j_{\mathcal{N}}$ serves as a direct proxy for the expected flight workload.

The assignment principle follows an intuitive matching strategy that cluster centers with larger $\bar{D}^j_{\mathcal{N}}$ values are assigned to SAR-UAVs with greater flight speeds V_i, which can be formally expressed as:

$$\bar{D}^j_{\mathcal{N}} > \bar{D}^k_{\mathcal{N}} \Rightarrow V_{i \to j} \geq V_{i \to k}, \tag{20}$$

where $i \to j$ denotes the SAR-UAV assigned to cluster center R_j.

The cluster center assignment phase ensures that SAR-UAVs with superior flight capabilities tend to handle clusters requiring greater mobility. Thus, the cluster center assignment phase is completed.

4.1.3. Region Clustering Phase

After assigning cluster centers to SAR-UAVs, the remaining regions must be grouped into appropriate clusters. Since each cluster center is already associated with a SAR-UAV that will execute the imaging tasks in its cluster, this phase aims to minimize mission completion time by optimally assigning regions to SAR-UAVs. Two critical considerations govern each region assignment:

- Residual energy sufficiency of candidate SAR-UAVs.
- Potential reduction in mission completion time.

As illustrated in Figure 3, regions are categorized as interior regions or edge regions. Specifically, a region is treated as an edge region if it lies on or outside the polygon hull formed by cluster centers; otherwise, it is treated as an interior region. Edge regions tend to have larger distances to cluster centers than interior regions. Since regions can only be assigned from clusters where SAR-UAVs have sufficient residual energy, late-stage assignments may force edge regions into distant clusters, thus incurring excessive mission completion time. To mitigate this issue, our strategy prioritizes assigning edge regions before interior regions. Two predictive metrics, predicted imaging time cost and predicted energy consumption, are introduced to guide SAR-UAV selection.

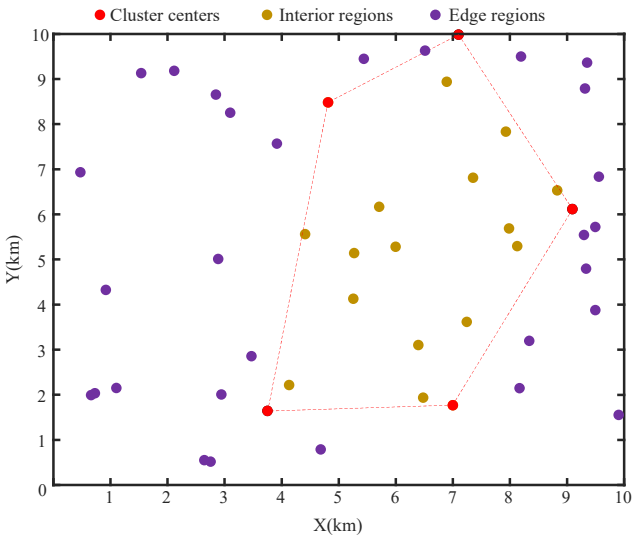


Figure 3. Illustration of edge region delineation based on the polygon hull formed by cluster centers ($N = 5$, $M = 50$).

For an unassigned region R_k, feasibility is checked by predicting the additional energy required. To ensure the assigned SAR-UAV has enough residual energy to fly back to the base after imaging R_k, the predicted energy consumption is conservatively estimated by assuming that each candidate SAR-UAV starts from the cluster center, images R_k, and returns to the base. Accordingly, for a candidate SAR-UAV U_i associated with cluster center R_j, the predicted time cost is

$$T_{\text{pre}}^{i,k} = \frac{D_{j,k} + D_{0,k}}{V_i} + \frac{S_k}{\kappa V_i W_i}, \tag{21}$$

and the predicted energy consumption is computed via

$$E_{\text{pre}}^{i,k} = P_i \cdot T_{\text{pre}}^{i,k}. \tag{22}$$

Only SAR-UAVs satisfying $E_{\text{res}}^{i,k-1} \geq E_{\text{pre}}^{i,k}$ are considered candidates, where $E_{\text{res}}^{i,k-1}$ denotes the residual energy of U_i before assigning the current unassigned region R_k with $k \in \{1, 2, \ldots, M\}$, which is defined as

$$E_{\text{res}}^{i,k-1} = E_{\max}^{i} - E_{\text{used}}^{i,k-1}, \tag{23}$$

where $E_{\text{used}}^{i,k-1}$ denotes the accumulated predicted energy consumption of U_i after processing the first $(k-1)$ region assignments. Specifically,

$$E_{\text{used}}^{i,k-1} = \sum_{m \in \mathcal{J}_{i,k-1}} E_{\text{pre}}^{i,m}, \tag{24}$$

with $\mathcal{J}_{i,k-1}$ denoting the set of regions assigned to U_i after the first $(k-1)$ assignments. The initialization is $E_{\text{used}}^{i,0} = 0$ and thus $E_{\text{res}}^{i,0} = E_{\max}^{i}$.

Finally, R_k will be assigned to one of the candidate SAR-UAVs that minimizes $T_{\text{pre}}^{i,k}$. This greedy criterion offers a computationally efficient heuristic to promote mission completion time reduction by prioritizing feasible assignments with lower time costs. Figure 4 demonstrates the clustering results for the scenario in Figure 3.

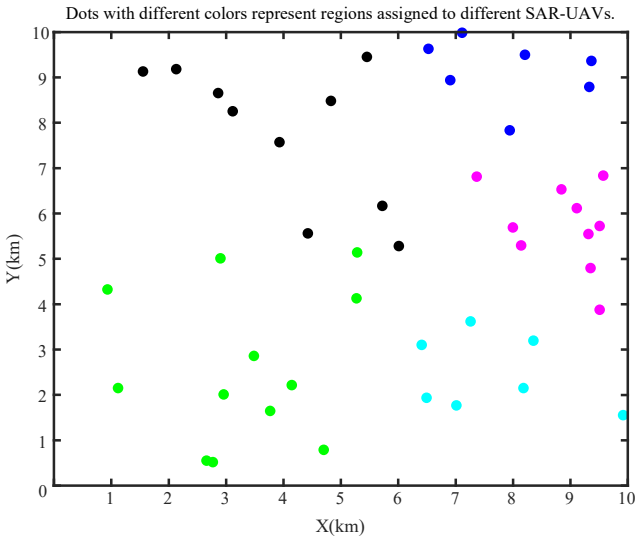


Figure 4. Clustering results of regions in Figure 3 (N = 5, M = 50).

4.1.4. Adaptively Triggered Distance-Based Clustering Strategy

While the ADCP strategy presented above performs well, its advantage may diminish in UAV-scarce scenarios where a limited number of SAR-UAVs must handle a large number of regions. As the number of regions assigned to an individual SAR-UAV increases, the flight-time component tends to become more influential, making the detailed area-density and cost-prediction clustering strategy less beneficial. Therefore, a simpler distance-based clustering is adopted to improve robustness.

Accordingly, an adaptive clustering strategy is introduced to identify UAV-scarce conditions according to the relationship between the number of ROIs and the number of available SAR-UAVs. When $N < \left\lfloor \frac{\sqrt{M}}{2} \right\rfloor$, the mission is regarded as a UAV-scarce scenario, and a nearest-eligible-center policy is activated to reduce excessive spatial dispersion while still satisfying the residual-energy constraint. While maintaining the edge-region-first assignment priority, regions are directly assigned to the closest cluster center whose assigned SAR-UAV has sufficient residual energy.

4.2. Path Planning via Discrete Secretary Bird Optimization

After assigning regions to SAR-UAVs, each SAR-UAV requires flight path planning to minimize mission completion time. The resulting path planning problem has a rapidly growing search space and is prone to local optima, thus requiring both sufficient global exploration and stable convergence behavior. The secretary bird optimization algorithm (SBOA) [43] features a distinctive multi-stage exploration mechanism and balanced exploration–exploitation search behavior, which enable it to maintain search diversity while reducing premature convergence. These characteristics make SBOA more suitable than geometric or conventional metaheuristic path generators for the considered path planning problem. Empirical studies demonstrate the effectiveness and efficiency of SBOA in multi-constrained path planning problems, exhibiting superior convergence speed and solution accuracy [44,45]. However, the direct application of SBOA to our formulated problem is limited by the discrete representation of paths as ordered waypoint sequences. To address this mismatch, a discrete adaptation of SBOA is designed for our problem context.

In our method, each candidate solution represents a candidate waypoint sequence. The continuous arithmetic operations in standard SBOA are replaced by a discrete mutation-based operator. Specifically, the former fundamental state update:

$$X^{\text{new}} = X + \mu \cdot X^{\text{target}} \tag{25}$$

is redefined in a probabilistic manner for waypoint-sequence optimization. In the discrete formulation, X denotes the current waypoint sequence, while X^{target} denotes the reference waypoint sequence generated by the corresponding SBOA update rule. The coefficient $\mu \in (0, 1)$ no longer represents an arithmetic step size, but is interpreted as the probability that each non-base waypoint in X participates in a position-exchange operation guided by X^{target}.

It should be noted that the proposed DSBOA still preserves the stage-wise search logic of the original SBOA. The proposed mutation operator provides a sequence-feasible discrete realization of the corresponding update direction. Therefore, DSBOA preserves the intended stage-wise transition from broader search to more localized refinement in a discrete form, rather than becoming an isolated mutation-driven heuristic. The specific procedure is described as follows.

As illustrated in Figure 5, the proposed mutation operator consists of three steps: decide, search, and mutate. In the decide step, each non-base waypoint in X independently determines whether to participate in mutation according to μ. Specifically, for each non-base waypoint, a random number $r \in [0, 1]$ is generated. If $r < \mu$, the waypoint is selected for mutation, otherwise it remains unchanged. In the search step, the position of the same ROI identifier in X^{target} is located for each selected waypoint. In the mutate step, the selected waypoint is swapped with the waypoint currently occupying the corresponding position in X. The selected waypoints are processed sequentially, so each position exchange is performed on the latest updated sequence until X^{new} is obtained. Since the operator only exchanges existing ROI identifiers within the sequence, it does not introduce duplicate or missing ROIs, thereby preserving waypoint-sequence feasibility.

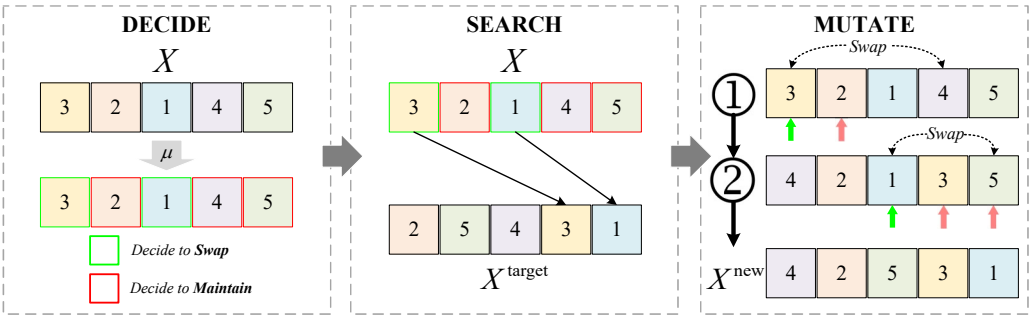


Figure 5. Illustrations of the mutation operator.

Before iterations, the population is initialized by random permutations of the assigned ROI indices, and fitness is evaluated by mission completion time. In each iteration, the population is sequentially updated through an exploration step followed by an exploitation step.

(1) Exploration Stage: In the exploration stage, the update rule is explicitly switched among three phases according to the ratio between the current iteration τ and the maximum number of iterations $\tau_{\max}$. Specifically, different exploration strategies are adopted in the early, middle, and late iterations to balance global search and local refinement.

During early iterations ($\tau < \frac{1}{3}\tau_{\max}$), a differential evolution strategy is employed to conduct extensive global exploration, aiming to rapidly converge toward the global optimum. Given an individual X_i, two candidates X_{r_1} and X_{r_2} are randomly selected to generate a new solution X_i^{new}, which can be calculated as:

$$X_i^{\text{new}} = X_i + \mu_1 \cdot (X_{r_1} + \mu_{e_1} \cdot X_{r_2}), \tag{26}$$

where $\mu_1 \sim \mathcal{U}(0, 1)$ is a uniform random variable, and $\mu_{e_1} \in (0, 1)$ is an empirical parameter. This phase can effectively enhance the global search capability of the population.

In middle iterations ($\frac{1}{3}\tau_{\max} \leq \tau < \frac{2}{3}\tau_{\max}$), the *Brownian* motion is integrated into the update process to further diversify the search and prevent premature convergence. Each solution is updated relative to its historical best solution X_{best}, which can be expressed via

$$X_i^{\text{new}} = X_{\text{best}} + \exp(\frac{\tau}{\tau_{\max}})^4 \cdot \mu_2 \cdot (X_{\text{best}} + \mu_{e_2} \cdot X_i), \tag{27}$$

where $\mu_2 \sim \mathcal{N}(0,1)$ is a standard normal random variable, with the same dimension as the solutions. $\mu_{e_2} \in (0,1)$ is an empirical constant.

During late exploration ($\tau \geq \frac{2}{3}\tau_{\max}$), the *Levy* flight model is introduced to generate step lengths characterized by a heavy-tailed distribution, facilitating a balanced search strategy. The state update for each candidate solution X_i follows:

$$X_i^{\text{new}} = X_{\text{best}} + \mu_L \cdot X_i, \tag{28}$$

where μ_L is the *Levy* flight parameter, which can be calculated according to [43]. The generated step lengths exhibit both occasional long-step exploration for global space coverage and frequent short-step refinement for local optimization accuracy.

(2) Exploitation Stage: After each exploration update, regardless of which exploration phase is currently active, one exploitation update is further performed. Specifically, either the camouflage by environment (CE) strategy or the fly or run (FR) strategy is randomly selected with equal probability to continue updating the candidate solution X_i, which can be calculated via:

$$X_i^{\text{new}} = \begin{cases} CE : X_{\text{best}} + \mu_{\text{CE}} \cdot X_i \\ FR : X_i + \mu_{e_3} \cdot (X_{r_3} + \mu_{\text{FR}} \cdot X_i), \end{cases} \tag{29}$$

where $\mu_{e_3} \in (0,1)$ is a constant, X_{r_3} denotes a randomly selected solution, and μ_{FR} is a discrete random variable taking values $\frac{1}{3}$ or $\frac{2}{3}$ with equal likelihood. The adaptive camouflage parameter μ_{CE} is defined as:

$$\mu_{\text{CE}} = (2 \cdot \mu_3 - 1) \cdot (1 - \frac{\tau}{\tau_{\max}})^2, \tag{30}$$

with $\mu_3 \sim \mathcal{N}(0,1)$ being another standard normal random variable.

For both exploration and exploitation stages, state updates occur conditionally as:

$$X_i = \begin{cases} X_i^{\text{new}} & \text{if } \mathcal{F}(X_i^{\text{new}}) < \mathcal{F}(X_i), \\ X_i & \text{otherwise} \end{cases} \tag{31}$$

where $\mathcal{F}(\cdot)$ denotes the fitness function, which is defined as the UAV mission time $T(Q_i)$. The optimization terminates upon reaching $\tau_{\max}$ iterations.

The discrete SBOA framework avoids the encoding–decoding overhead of existing metaheuristic-based path planning methods while preserving solution feasibility. Elitist propagation of high-fitness solutions accelerates convergence by minimizing redundant search. The proposed approach differs structurally from conventional metaheuristics [26,31,46] by replacing arithmetic calculations with mutation operations, thereby eliminating solution mapping errors while adaptively incorporating heterogeneous UAV constraints. The generated paths for clustered regions in Figure 4 are shown in Figure 6. Note that the circles in Figure 6 are only used to visualize the associated imaging workloads of regions, rather than representing the actual shapes of the target regions in the mission.

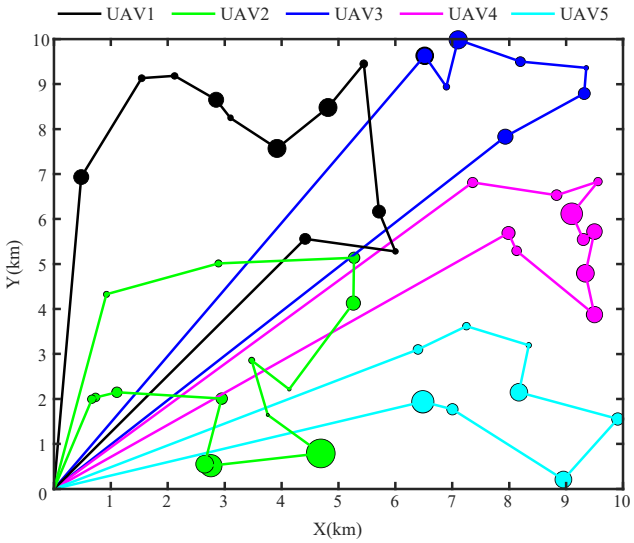


Figure 6. Generated paths for clustered regions in Figure 4 ($N = 5$, $M = 50$).

The main algorithmic framework of the proposed joint task assignment and path planning method is outlined in Algorithm 1.

Algorithm 1: Joint Task Assignment and Path Planning for Heterogeneous SAR-UAVs.

Input: UAV set U, region set R, distance matrix D
Output: Paths $Q = \{Q_1, \ldots, Q_N\}$
Stage 1: Task Assignment via ADCP
Cluster-center selection:
foreach *region* R_j **do**
  Compute imaging workload ρ_j, distance factor δ_j;
  Compute selection metric $\gamma_j = \rho_j \delta_j$;
Select N regions with largest γ_j as initial cluster center set $\mathcal{C}$;
Cluster center assignment:
foreach *cluster center* $c_j \in \mathcal{C}$ **do**
  Estimate KNN-based flight workload $\bar{D}^j_{\mathcal{N}}$;
Sort centers by $\bar{D}^j_{\mathcal{N}}$ and SAR-UAVs by flight speed;
Assign each cluster center c_j to SAR-UAV U_i by ranking-based matching between workload $\bar{D}^j_{\mathcal{N}}$ and UAV flight speeds;
Region clustering:
Initialize cluster center for each SAR-UAV U_i;
if $N < \left\lfloor \frac{\sqrt{M}}{2} \right\rfloor$ **then**
  Reassign each region to the nearest feasible center;
else
  foreach *unassigned region* R_k **do**
    foreach *SAR-UAV* U_i **do**
      Predict time cost $T^{i,k}_{\text{pre}}$;
      Predict energy consumption $E^{i,k}_{\text{pre}} = P_i \cdot T^{i,k}_{\text{pre}}$;
      if $E^{i,k}_{pre} \leq E^{i,k-1}_{res}$ **then**
        Mark U_i as feasible for R_k;
    Assign R_k to the feasible SAR-UAV with minimum $T^{i,k}_{\text{pre}}$;
Coupling mechanism: The resulting clusters define the region set required to be imaged by each SAR-UAV in the **Stage 2**;
Stage 2: Path Planning via DSBOA
foreach *SAR-UAV* U_i **do**
  Generate an initial population from the assigned cluster of U_i;
  for $\tau = 1$ **to** $\tau_{\max}$ **do**
    Evaluate fitness $T(Q_i)$;
    Select an exploration strategy based on $\frac{\tau}{\tau_{\max}}$;
    Randomly select an exploitation strategy from $\{CE, FR\}$ with equal probability;
    Update the population using the discrete mutation operator;
  Select best individual as path Q_i;
return $Q = \{Q_1, \ldots, Q_N\}$

5. Time Complexity Analysis

This subsection analyses the time complexity of the proposed ADCP clustering strategy and DSBOA path planning method.

The proposed ADCP approach consists of three phases: cluster center selection, cluster center assignment, and region clustering. In the cluster center selection phase, calculating the imaging workload ρ and relative distance factor δ for all regions each requires $O(M^2)$ operations. Thus, this phase exhibits $O(M^2)$ complexity. In the second phase, constructing the KNN sets for N cluster centers by finding their nearest neighbors among M regions requires $O(N \cdot M)$ operations. In calculating $\bar{D}^j_{\mathcal{N}}$ in Equation (18), each neighbor in the K-sized KNN set computes its minimum distance to M regions. Therefore, N cluster centers require $O(N \cdot K \cdot M)$ operations. The UAV-cluster assignment is of $O(N \cdot \log N)$ complexity. With $K = \lfloor M/N \rfloor$, the dominant term in the cluster center assignment phase is $O(N \cdot K \cdot M) = O(M^2)$. The main procedure of the region clustering phase requires $O(N \cdot M)$ operations and the nearest-eligible-center policy in the adaptive clustering strategy requires $O(N \cdot M)$ operations when activated. In summary, the overall time complexity is dominated by the $O(M^2)$ term, as $N \ll M$ in practical applications.

The time complexity of the proposed path planning method is analyzed below. It consists of two phases: population initialization and population updating. Let N_{pop} denote the population size, and the dimensionality of each secretary bird is equal to the number of regions M. Randomly initializing the population requires $O(N_{\text{pop}})$ operations. During the population updating process, the complexity is dominated by $O(N_{\text{pop}} \cdot I_{\max} \cdot M)$, derived from the terms $O(N_{\text{pop}} \cdot I_{\max})$ and $O(N_{\text{pop}} \cdot I_{\max} \cdot M)$. Consequently, the computational complexity of the proposed path planning approach simplifies to $O(N_{\text{pop}} \cdot I_{\max} \cdot M)$.

Combining the above analyses, the overall time complexity of the proposed method is $O(M^2) + O(N_{\text{pop}} \cdot I_{\max} \cdot M)$. This expression establishes that computational cost depends on the number of regions M, population size N_{pop}, and the maximum number of iterations $I_{\max}$. Thus, the proposed method exhibits polynomial-time complexity with respect to M given fixed N_{pop} and $I_{\max}$. Although scalability is constrained by M, the empirical results show that the proposed method remains computationally tractable for minimizing SAR-UAV mission completion time.

6. Simulation Results

Simulations under varied parameter configurations are conducted to evaluate the effectiveness of the proposed joint task assignment and path planning method. First, comparative benchmarking results under parametric variations are analyzed. Then, ablation experiments of the ADCP clustering strategy and the DSBOA path planning method are conducted. Finally, some additional observational findings are presented.

In our experiments, target regions are randomly distributed within a 10,000 m $\times$ 10,000 m mission area. Following [24,31], the sizes of target regions are generated using the Unnifast algorithm [47] with a utilization factor uti which is defined as:

$$\text{uti} = \frac{\sum_{i=1}^{M} S_i}{S_{\text{total}}}. \tag{32}$$

All simulations were conducted over 1000 Monte Carlo trials on an Intel(R) Core(TM) i9-12900K 3.19 GHz processor utilizing the MATLAB R2022b platform. Simulation parameters are detailed in Table 1.

Table 1. Simulation parameters.

Parameters	Value
Number of SAR-UAVs	{3, 4, 5, 6, 7, 8, 9}
Number of regions	{50, 60, 70, 80, 90, 100, 110, 120}
Flight altitude (m)	120
SAR side-looking angle (°)	35
Flight speed (m/s)	5∼15
SAR vertical beamwidth (°)	0.5∼2
Utilization factor	{0.0005, 0.0010, 0.0015, 0.0020, 0.0025}
Maximum iteration number	100
Population size	30

6.1. Performance Evaluation

In this subsection, the performance of the proposed method is benchmarked against four representative approaches: the spatial–temporal clustering-based algorithm with nearest-to-all strategy (STCA_NA) proposed in [24], the genetic algorithm based on K-means (Kmeans_GA) presented in [46], the particle swarm optimization algorithm (PSO) adopted in [31], and the ant colony optimization method (ACO) in [20]. STCA_NA has been widely regarded as a representative joint task assignment and path planning method for heterogeneous UAVs [13,48]. Kmeans_GA adopts a dual-stage framework combining K-means clustering and a genetic algorithm (GA), both of which are long-standing benchmark methods in clustering and heuristic optimization [49]. ACO and PSO are well-established swarm intelligence methods and commonly used baselines in related studies [50].

Since the above approaches were originally developed for the same category of path planning problems as our approach, i.e., minimizing mission completion time or the corresponding flight-path length, the mission completion time and average CPU computation time of the proposed method and all baselines are evaluated across parameter variations.

Before comparing the proposed method with the representative baselines, the sensitivity of the cut-off distance d_c is first evaluated to verify that the adopted parameter setting does not dominate the reported performance. As shown in Table 2, varying the percentile coefficient η_c from 0.05 to 0.09 leads to moderate changes in mission completion time around the nominal setting $\eta_c = 0.07$. This range follows the percentile-based local-neighborhood selection practice commonly used in density peak clustering [24,31]. The maximum relative change is 10.43%, which occurs at $\eta_c = 0.09$. These results indicate that the proposed ADCP strategy maintains stable performance within a representative local-neighborhood range, rather than relying on a single manually selected cut-off distance.

Table 2. Sensitivity analysis of the cut-off distance percentile under the representative setting (M = 100, N = 5, uti = 0.0005).

η_c	Mission Completion Time (s)	Relative Change (%)
0.05	5.85×10^3	+5.22
0.06	5.67×10^3	+1.98
0.07	5.56×10^3	–
0.08	5.84×10^3	+5.04
0.09	5.94×10^3	+6.83

Figure 7 compares the mission completion time distributions of five methods. All approaches exhibit increasing mission completion times as the number of regions grows from 50 to 120, since more regions generally lead to longer traversal distances. The proposed method consistently exhibits the lowest mission completion time distribution across all

settings. Specifically, when the number of regions M = 90, the proposed method achieves an average mission completion time of 5625 s, which is 30%, 22%, 47%, and 23% less than that of STCA_NA, Kmeans_GA, PSO, and ACO, respectively. Furthermore, the proposed method exhibits significantly enhanced performance stability, with an interquartile range up to 48.6% narrower than those of the comparative methods. These performance gains mainly stem from the explicit consideration of both flight workload and SAR imaging workload in the ADCP method, which enables more effective matching between ROI demands and heterogeneous SAR-UAV capabilities as the number of regions increases.

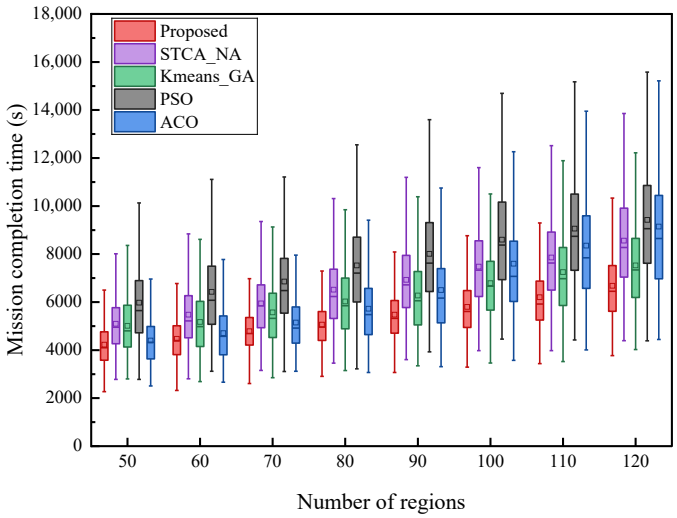


Figure 7. Mission completion times (in seconds) when different numbers of regions were covered (N = 5, uti = 0.0005).

Figure 8 presents the mission completion times when varying the number of SAR-UAVs. While all methods benefit from distributed workload, the proposed method maintains superior performance and stable distribution throughout the scalability range. Although increasing the number of SAR-UAVs improves assignment flexibility, it also amplifies the influence of assignment quality on workload imbalance. In the proposed method, ROI workloads are more effectively matched with heterogeneous UAV flight and imaging capabilities, so the observed performance gain essentially stems from this capability-aware assignment.

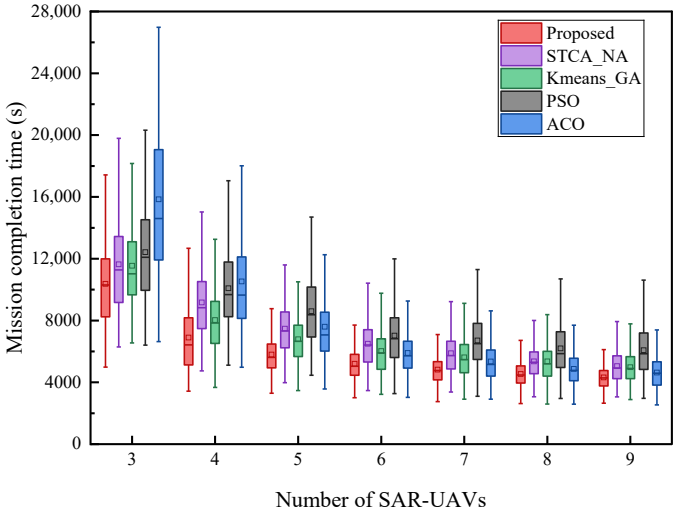


Figure 8. Mission completion times (in seconds) when different numbers of SAR-UAVs were adopted (M = 100, uti = 0.0005).

Table 3 reports the mean and standard deviation of individual UAV mission completion times under different numbers of SAR-UAVs. The distribution of individual UAV mission completion times provides a direct measure of workload balance in the parallel heterogeneous mission. It can be observed that the proposed method consistently achieves the lowest mean per-UAV mission completion time, together with the smallest standard deviation across almost all tested settings. These results verify the effectiveness of the proposed method in improving workload balance at the system level, which underlies the performance gain of the proposed method observed in Figure 8.

Table 3. Mean and standard deviation of per-UAV mission completion time (in seconds) under different numbers of SAR-UAVs (M = 100, uti = 0.0005).

Number of SAR-UAVs	Statistics	Proposed	STCA_NA	Kmeans_GA	PSO	ACO
3	Avg	7.86×10^3	8.99×10^3	7.86×10^3	9.36×10^3	9.67×10^3
	(±Std Dev)	($\pm 2.13 \times 10^3$)	($\pm 2.16 \times 10^3$)	($\pm 2.22 \times 10^3$)	($\pm 3.26 \times 10^3$)	($\pm 2.27 \times 10^3$)
4	Avg	5.41×10^3	6.53×10^3	5.46×10^3	6.17×10^3	6.93×10^3
	(±Std Dev)	($\pm 1.70 \times 10^3$)	($\pm 1.86 \times 10^3$)	($\pm 1.75 \times 10^3$)	($\pm 2.63 \times 10^3$)	($\pm 2.08 \times 10^3$)
5	Avg	4.08×10^3	5.15×10^3	4.26×10^3	4.50×10^3	5.57×10^3
	(±Std Dev)	($\pm 1.24 \times 10^3$)	($\pm 1.60 \times 10^3$)	($\pm 1.62 \times 10^3$)	($\pm 1.74 \times 10^3$)	($\pm 1.94 \times 10^3$)
6	Avg	3.36×10^3	4.35×10^3	3.65×10^3	3.67×10^3	4.40×10^3
	(±Std Dev)	($\pm 1.19 \times 10^3$)	($\pm 1.46 \times 10^3$)	($\pm 1.46 \times 10^3$)	($\pm 1.38 \times 10^3$)	($\pm 1.72 \times 10^3$)
7	Avg	2.91×10^3	3.72×10^3	3.21×10^3	3.08×10^3	3.93×10^3
	(±Std Dev)	($\pm 1.14 \times 10^3$)	($\pm 1.27 \times 10^3$)	($\pm 1.37 \times 10^3$)	($\pm 1.17 \times 10^3$)	($\pm 1.61 \times 10^3$)
8	Avg	2.70×10^3	3.35×10^3	2.93×10^3	2.76×10^3	3.35×10^3
	(±Std Dev)	($\pm 1.08 \times 10^3$)	($\pm 1.15 \times 10^3$)	($\pm 1.32 \times 10^3$)	($\pm 1.11 \times 10^3$)	($\pm 1.46 \times 10^3$)
9	Avg	2.38×10^3	2.97×10^3	2.66×10^3	2.48×10^3	3.15×10^3
	(±Std Dev)	($\pm 9.92 \times 10^2$)	($\pm 1.06 \times 10^3$)	($\pm 1.29 \times 10^3$)	($\pm 1.13 \times 10^3$)	($\pm 1.35 \times 10^3$)

Table 4 reports the mean and standard deviation of per-UAV residual energy under different numbers of SAR-UAVs. It can be observed that the proposed method generally achieves higher or competitive mean per-UAV residual energy than the comparative methods across the tested settings. The non-minimal standard deviation of residual energy is consistent with the objective setting of the present formulation, where energy balance is not explicitly optimized. Meanwhile, these results demonstrate the positive role of the residual energy sufficiency evaluation in the final clustering process, as it helps avoid assigning ROI clusters to UAVs with insufficient remaining energy and thereby preserves energy feasibility.

Table 4. Mean and standard deviation of per-UAV residual energy (%) under different numbers of SAR-UAVs (M = 100, uti = 0.0005).

Number of SAR-UAVs	Statistics	Proposed	STCA_NA	Kmeans_GA	PSO	ACO
3	Avg	25.25	13.20	24.71	7.51	9.90
	(±Std Dev)	(±26.65)	(±16.69)	(±13.93)	(±40.99)	(±13.91)
4	Avg	48.54	38.69	48.35	40.01	34.11
	(±Std Dev)	(±19.78)	(±14.03)	(±11.21)	(±24.22)	(±13.24)
5	Avg	60.04	50.81	59.68	57.50	49.02
	(±Std Dev)	(±16.42)	(±11.34)	(±11.27)	(±12.05)	(±11.38)
6	Avg	66.18	59.45	66.14	66.52	59.79
	(±Std Dev)	(±15.37)	(±10.23)	(±10.43)	(±9.28)	(±10.01)
7	Avg	70.09	64.84	69.66	70.06	63.05
	(±Std Dev)	(±12.98)	(±9.41)	(±9.12)	(±8.75)	(±10.70)
8	Avg	73.31	67.76	72.60	73.73	68.11
	(±Std Dev)	(±12.20)	(±9.40)	(±9.05)	(±7.87)	(±10.45)
9	Avg	74.66	70.47	74.64	75.83	69.36
	(±Std Dev)	(±11.05)	(±9.33)	(±8.91)	(±7.88)	(±10.41)

Figure 9 compares mission completion times under different system utilization factors uti. As uti increases, corresponding to higher imaging workloads, all methods experience progressive performance degradation. As defined in Equations (1) and (5)–(7), mission completion time consists of imaging time and flight time, uti directly determines the total area required for imaging. As this area increases, imaging time becomes the dominant component of mission completion time, reducing the relative influence of flight-time-related optimization. Consequently, under high utilization, the performance of all approaches is primarily governed by the SAR vertical beamwidths. Nonetheless, the proposed method still demonstrates superior performance. This residual advantage still comes from the explicit introduction of imaging workload and its effective role in workload-to-capability matching, which remains beneficial when imaging time dominates mission completion time.

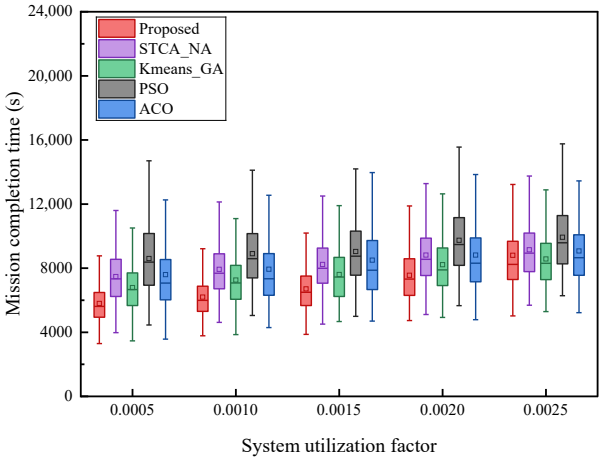


Figure 9. Mission completion times (in seconds) when regions were generated by different system utilization factors (N = 5, M = 100).

6.2. Computation Time Evaluation

The computational efficiency of the five approaches is evaluated using the average CPU time required to generate feasible SAR-UAV paths.

Figure 10 demonstrates an approximately linear increase in average CPU computation time with increasing regions from 50 to 120, consistent with our time complexity analysis in Section 5. While the proposed method does not achieve the lowest CPU time, its near-linear scaling with M indicates favorable computational scalability.

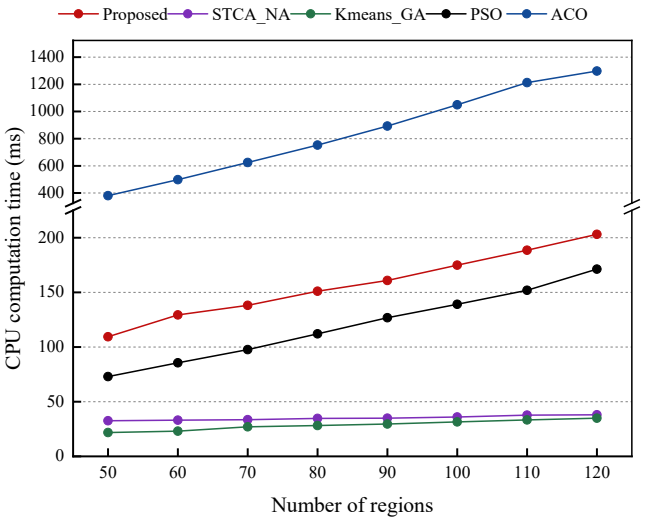


Figure 10. Average CPU computation times (in milliseconds) when different numbers of regions were covered (N = 5, uti = 0.0005).

Table 5 further reports the component-wise CPU times of different task assignment approaches and path planning methods. It can be observed that the DSBOA iterations dominate the computational cost of our method, accounting for 87–91% of the total computation time. Although not achieving minimal CPU computation times, the proposed ADCP clustering strategy and DSBOA path planning method remain practical with moderate absolute computational times and favorable scalability.

Table 5. Average CPU computation times (in milliseconds) of task assignment approaches and path planning methods when different numbers of regions were covered (N = 5, uti = 0.0005).

Number of Regions	ADCP	Kmeans	DPC	STCA	DSBOA	GA	PSO	ACO
50	14.68	10.02	2.79	3.27	94.71	70.15	21.58	380.47
60	15.53	10.03	2.94	3.97	110.82	82.66	22.15	498.26
70	16.23	10.93	3.12	4.39	121.94	94.58	22.64	624.66
80	16.96	11.15	3.15	5.11	134.20	108.95	23.57	752.76
90	16.77	11.49	3.31	5.62	144.16	123.51	23.96	892.74
100	16.86	11.55	3.39	7.08	158.02	135.74	24.47	1049.22
110	17.13	12.13	3.44	7.77	171.43	148.47	25.62	1212.36
120	18.39	12.16	3.87	9.06	184.69	167.39	25.90	1297.84

In Figure 11, our proposed method exhibits an approximately linear increase in average CPU time as the number of SAR-UAVs grows. According to the analysis in Section 5, the CPU runtime of the proposed method is not expected to increase with N. However, paths are generated independently for each SAR-UAV in practical implementations, which introduces a per-UAV fixed overhead and leads to a slight increase in CPU time. ACO shows a different trend, with a non-monotonic change because the reduced number of regions assigned to each UAV offsets the additional multi-UAV overhead when $N > 5$.

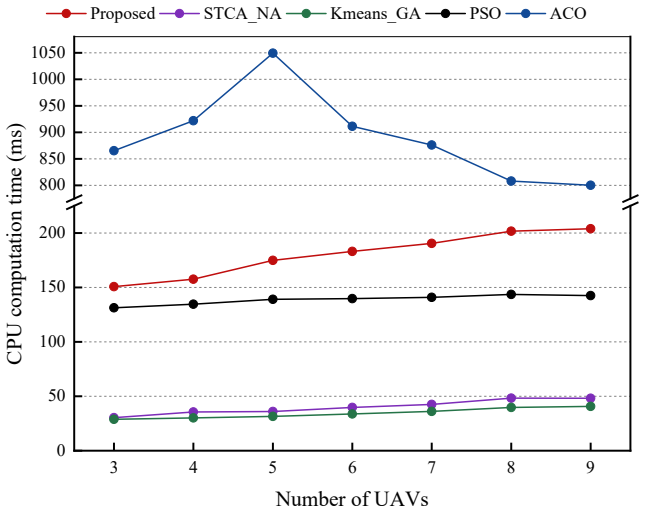


Figure 11. Average CPU computation times (in milliseconds) when different numbers of SAR-UAVs were adopted (M = 100, uti = 0.0005).

In summary, while the proposed method exhibits slightly higher computational demands compared to some of the baselines, its efficiency is sufficient to accommodate the computational requirements of a wide range of real-world application scenarios, affirming the practical utility of the proposed method.

6.3. Ablation Evaluation of Task Assignment Methods

This subsection evaluates the mission completion time of different task assignment methods integrated with the proposed DSBOA path planner. Three benchmark strategies are compared: the spatial–temporal clustering algorithm (STCA) proposed in [24], the K-means algorithm employed in [46], and the density peak clustering (DPC) algorithm utilized in [31].

Figure 12 shows the mission completion times across varying numbers of regions with a fixed number of SAR-UAVs. The proposed ADCP method consistently achieves superior performance, reducing average mission completion times by 5–14% compared with the benchmark method STCA. This significant improvement persists regardless of workload variations, indicating the robustness of our clustering strategy in generating optimal region clustering results. This advantage mainly comes from introducing both area density and cost prediction into the assignment process, so that the generated ROI clusters better reflect the actual mission-time contribution of different regions and reduce workload mismatch among heterogeneous SAR-UAVs.

According to the analysis in Section 4.1.4 and preliminary experimental observations, the performance advantage of the ADCP method without the adaptive clustering strategy diminishes when fewer than five SAR-UAVs are deployed. Figure 13 further evaluates the scalability of the proposed ADCP method after introducing the adaptive clustering strategy. The proposed method maintains competitive performance, and when the number of SAR-UAVs exceeds four, it regains clear dominance. In particular, it achieves up to a 9% reduction in mission completion time compared with the best-performing benchmark, K-means, at $N = 5$. The adaptive clustering strategy is introduced to better handle UAV-scarce conditions, where the assignment becomes more sensitive to the trade-off between workload awareness and spatial compactness. It therefore helps preserve effective ROI-to-UAV matching across different SAR-UAV fleet sizes.

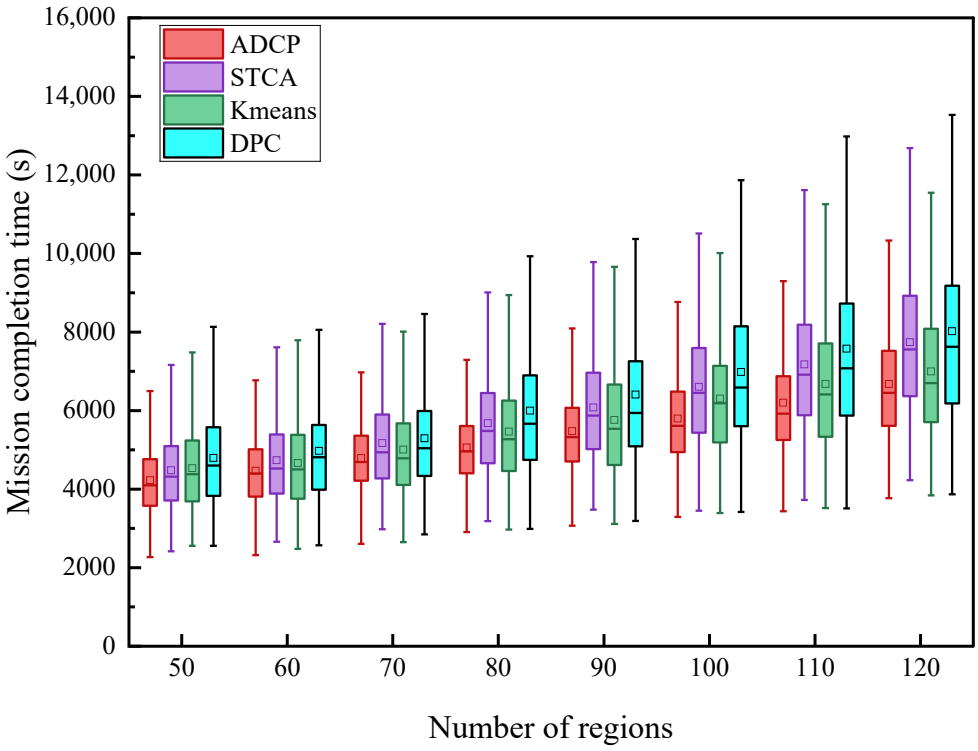


Figure 12. Mission completion times (in seconds) of task assignment approaches with DSBOA when different numbers of regions were covered (N = 5, uti = 0.0005).

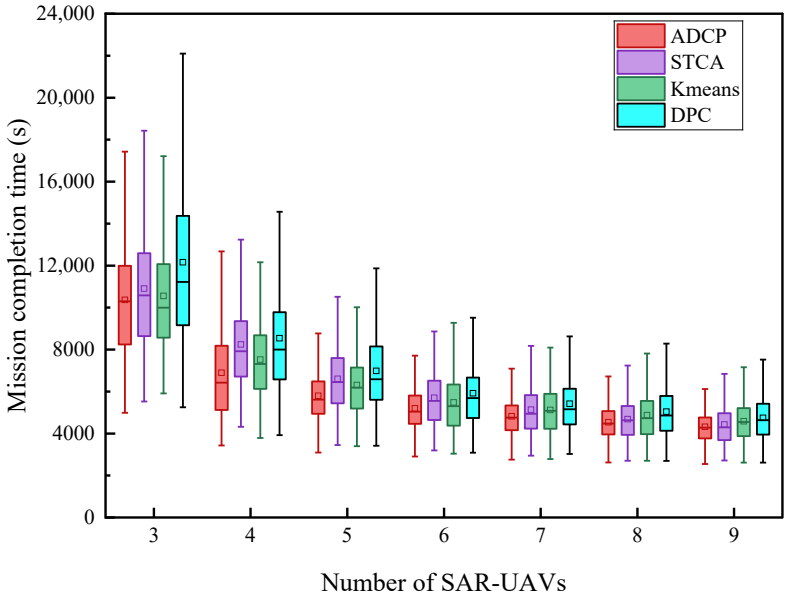


Figure 13. Mission completion times (in seconds) of task assignment approaches with DSBOA when different numbers of SAR-UAVs were adopted (M = 100, uti = 0.0005).

6.4. Ablation Evaluation of Path Planning Methods

In simulations of Figures 14 and 15, the mission completion times for different metaheuristic-based path planning methods integrated with the ADCP task assignment strategy are evaluated. Comparative benchmarks include ant colony optimization (ACO) from [20], particle swarm optimization (PSO) in [31], and the genetic algorithm (GA) from [46]. In addition, an additional mutation-driven discrete heuristic (MDH) is introduced as an ablation baseline to further verify that the effectiveness of DSBOA does not come merely from the proposed mutation-based operator. In the MDH method, the same discrete waypoint representation and sequence-feasible mutation operator are retained, while the SBOA-guided reference-sequence generation and the corresponding stage-wise search logic are removed. Instead, the mutation-based operator is applied with a fixed mutation probability using a random reference sequence.

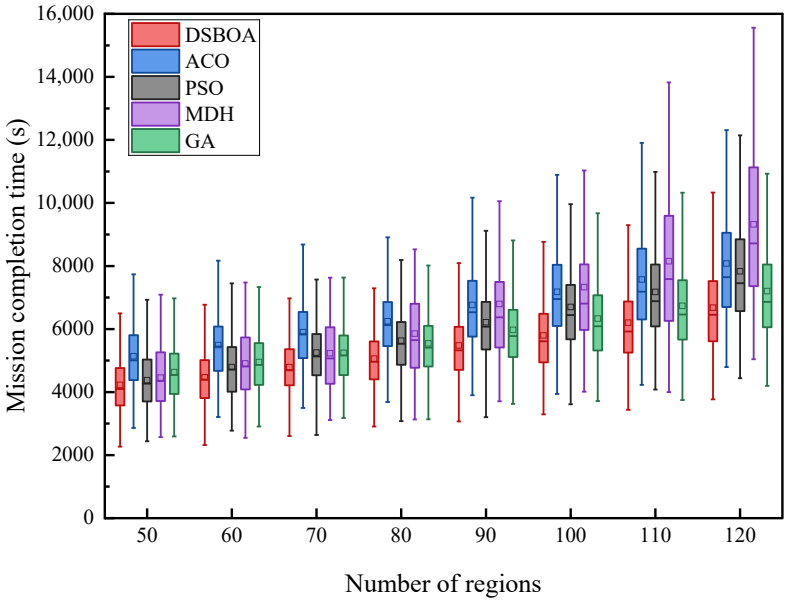


Figure 14. Mission completion times (in seconds) of metaheuristics with ADCP when different numbers of regions were covered (N = 5, uti = 0.0005).

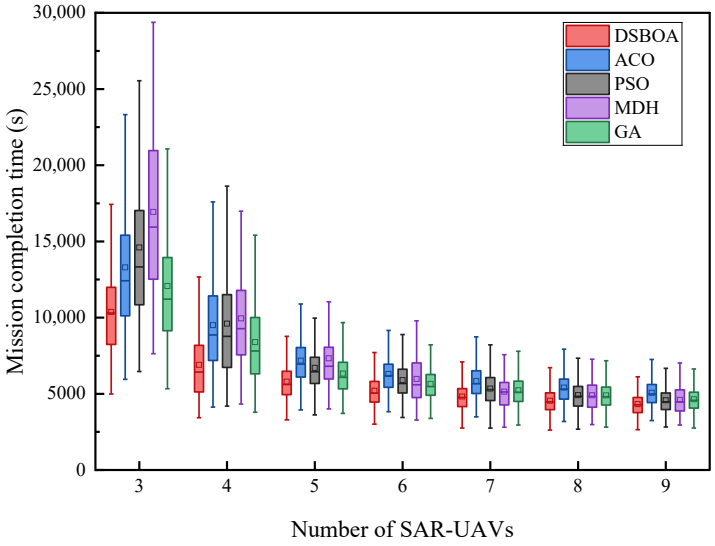


Figure 15. Mission completion times (in seconds) of metaheuristics with ADCP when different numbers of SAR-UAVs were adopted (M = 100, uti = 0.0005).

Figure 14 demonstrates that the proposed DSBOA path planner consistently achieves the lowest average mission completion times across all numbers of regions. The proposed DSBOA path planner exhibits the narrowest interquartile range in the box plot analysis, indicating superior performance robustness. As shown in Figure 15, the significant performance advantages persist when varying the number of SAR-UAVs. Overall, the proposed DSBOA path planning method consistently demonstrates superior effectiveness and robustness. This advantage mainly stems from the fact that DSBOA directly operates on discrete waypoint sequences and uses a specialized mutation mechanism to preserve sequence feasibility while enhancing search diversity, thereby enabling more effective exploration of high-quality visiting orders than the benchmark metaheuristics. Moreover, the superior performance of the proposed method over the MDH variant further confirms that the effectiveness of DSBOA does not come merely from the mutation operator itself. Instead, it comes from preserving the intended SBOA-inspired search characteristics in a discrete form, which enables a more effective transition from broader search to localized refinement during the visiting-sequence optimization process.

Convergence results in Table 6 show that the convergence time of all methods increases as the number of regions grows, indicating the higher combinatorial complexity induced by larger problem sizes. Notably, the average convergence time of DSBOA remains consistently lower than that of ACO, PSO, MDH, and GA across all region counts. Table 7 further evaluates the impact of the number of SAR-UAVs under a fixed number of regions. As N increases, the convergence time decreases for all methods due to the reduced regions-per-UAV workload. DSBOA maintains the fastest convergence, achieving a 50–78% reduction in convergence time compared with the baselines. This accelerated convergence stems from the combination of discrete waypoint sequence representation with the specialized mutation operator, which enhances population diversity and global search efficiency throughout the evolutionary process. As a result, DSBOA can reach high-quality visiting sequences more quickly within the same iteration budget, thereby contributing to its superior final path performance. Moreover, the significantly faster convergence of DSBOA compared with MDH further confirms that DSBOA preserves the intended SBOA-inspired stage-wise search characteristics in a discrete form.

Table 6. Average convergence times when different numbers of regions were covered (N = 5, uti = 0.0005).

Number of Regions	ACO	PSO	GA	MDH	DSBOA
50	30.8	52.5	52.0	48.9	11.6
60	38.5	63.5	62.2	60.6	14.3
70	41.5	71.1	69.3	67.4	16.6
80	44.6	77.4	75.1	75.1	18.6
90	46.9	82.6	80.8	77.3	20.6
100	48.8	85.7	84.0	81.6	22.5
110	49.8	87.8	86.8	84.3	23.8
120	50.0	90.5	88.8	85.5	25.3

Table 7. Average convergence times when different numbers of SAR-UAVs were adopted (M = 100, uti = 0.0005).

Number of SAR-UAVs	ACO	PSO	GA	MDH	DSBOA
3	51.8	90.1	91.9	90.0	27.4
4	49.8	89.9	90.4	89.3	25.3
5	48.8	85.7	84.0	81.6	22.5
6	43.0	76.8	75.0	73.4	18.9
7	39.6	68.3	65.9	64.5	16.4
8	34.3	60.7	59.2	59.0	14.7
9	32.9	53.9	52.7	53.0	12.7

6.5. Additional Findings

In this subsection, the total mission times (sum of per-UAV mission completion times) of joint task assignment and path planning approaches are analyzed. This measure is not used as a performance comparison metric and does not affect the comparative evaluation of the proposed method. Instead, it provides a complementary view of the overall mission workload and its trend is closely related to the total propulsion energy, which can be computed as

$$E_{\text{tot}} = \sum_{i=1}^{N} P_i \cdot T(Q_i). \tag{33}$$

Our analysis reveals two significant patterns across different parameter settings.

Figure 16 demonstrates that the proposed method achieves the minimal total mission time across all numbers of regions. This advantage persists consistently under varying region sizes, as evidenced in Figure 17. The above experimental results confirm that the proposed method is effective as a robust energy optimization framework for various imaging tasks.

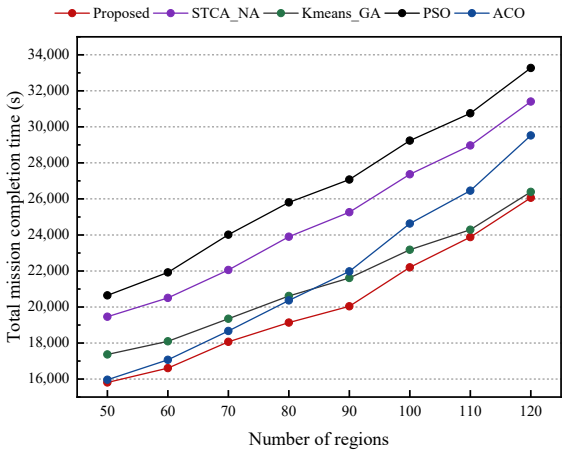


Figure 16. Average total mission times (in seconds) when different numbers of regions were covered (N = 5, uti = 0.0005).

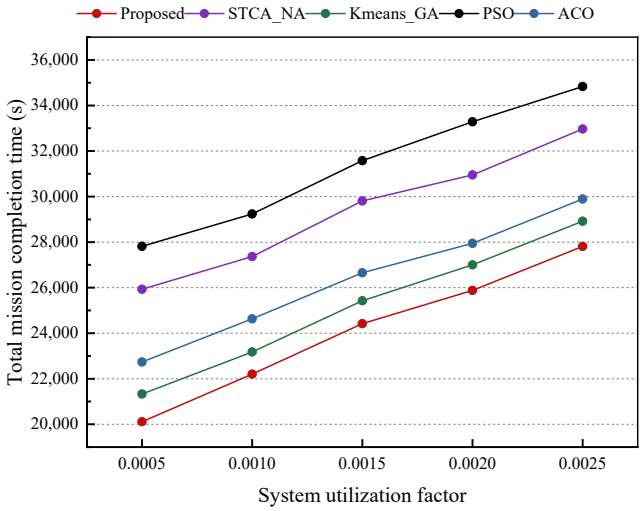


Figure 17. Average total mission times (in seconds) when regions were generated by different system utilization factors (N = 5, M = 100).

However, Figure 18 reveals a U-shaped profile. The proposed method achieves the minimum total mission time at N = 6, with reductions of 16% and 10% compared with N = 3 and N = 9, respectively. These U-shaped curves manifest the radial-local travel trade-off. Under-provisioning ($N < 6$) exacerbates local path complexity through elevated per-UAV task density, while over-provisioning ($N \geq 6$) dominates total flight distance due to excessive radial base-to-region transits.

This finding confirms the existence of an energy-optimal number of SAR-UAVs for the multi-region imaging mission. The proposed approach provides an empirical basis for jointly considering path planning and SAR-UAV fleet-size selection when reducing total energy consumption.

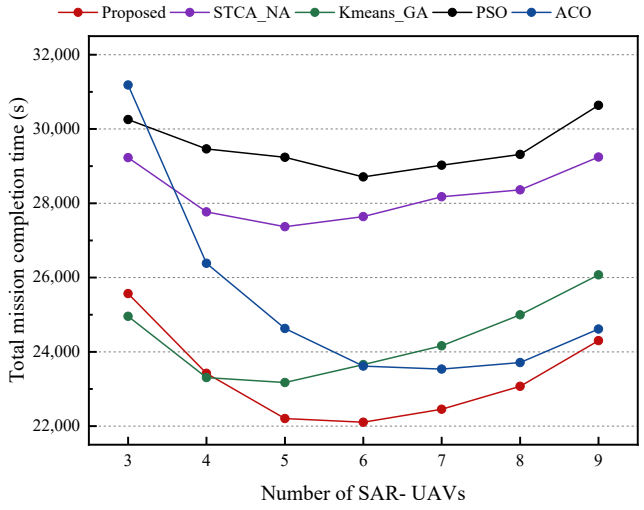


Figure 18. Average total mission times (in seconds) when different numbers of SAR-UAVs were adopted (M = 100, uti = 0.0005).

7. Conclusions

This article addresses the joint task assignment and path planning problem for heterogeneous SAR-UAVs in multi-region imaging missions, with the objective of improving mission time efficiency. First, by considering practical energy, imaging, and mission constraints, a joint optimization model is established to minimize the mission completion time. Then, an improved clustering strategy ADCP is proposed to match ROI-dependent

workloads with heterogeneous SAR-UAV capabilities during task assignment, thereby improving assignment quality. In addition, an adaptively triggered distance-based clustering strategy is introduced to enhance robustness under UAV-scarce conditions. For path planning, the DSBOA method is developed to determine the visiting order for each SAR-UAV. Convergence efficiency is enhanced through discrete solution representation and a specialized mutation-based operator.

The proposed method can generate high-quality feasible solutions for heterogeneous SAR-UAVs with tractable computational cost, thereby improving the information acquisition efficiency of SAR-UAV systems. Extensive simulations demonstrate that the proposed method consistently outperforms representative benchmark approaches in mission completion time under different parameter settings, while also exhibiting favorable scalability. Ablation experiments further verify the effectiveness of both the proposed ADCP task assignment strategy and the DSBOA path planning method.

Future work will extend the proposed method to incorporate more practical operational constraints and sensing requirements. For instance, some ROIs necessitate specific sensor payloads or collaborative sensing configurations for high-quality imaging, which will further motivate the joint optimization of task assignment, path planning, and UAV formation in heterogeneous SAR-UAV systems.

Author Contributions: Conceptualization, X.Z.; Formal analysis, X.Z.; Methodology, D.S.; Software, D.S.; Validation, D.S.; Writing—original draft preparation, B.W.; Investigation, Y.Z.; Resources, Y.Z.; Data curation, Y.Y.; Writing—review and editing, K.Q. All authors have read and agreed to the published version of the manuscript.

Funding: This work was supported by the Sichuan Natural Science Foundation (General Program) under Grant 2024NSFSC0176.

Data Availability Statement: The original contributions presented in the study are included in the article. Further inquiries can be directed to the corresponding author.

Conflicts of Interest: The authors declare no conflicts of interest.

References

1. Wang, L.; Zhang, X.; Qin, K.; Wang, Z.; Zhou, J.; Song, D. AoI Analysis of Satellite–UAV Synergy Real-Time Remote Sensing System. *Remote Sens.* **2024**, *16*, 3305. [CrossRef]
2. Collignon, M.; Perrusquía, A.; Tsourdos, A.; Guo, W. Search and rescue operations in wildfires using unmanned aerial vehicles: A multi-agent deep reinforcement learning approach. *Neurocomputing* **2025**, *643*, 131211. [CrossRef]
3. Liu, X.; Li, G.; Yang, H.; Zhang, N.; Wang, L.; Shao, P. Agricultural UAV trajectory planning by incorporating multi-mechanism improved grey wolf optimization algorithm. *Expert Syst. Appl.* **2023**, *233*, 120946. [CrossRef]
4. Xu, S.; Zhou, Z.; Liu, H.; Zhang, X.; Li, J.; Gao, H. A Path Planning Method for Collaborative Coverage Monitoring in Urban Scenarios. *Remote Sens.* **2024**, *16*, 1152. [CrossRef]
5. Li, J.; Yang, X.; Yang, Y.; Liu, X. Cooperative mapping task assignment of heterogeneous multi-UAV using an improved genetic algorithm. *Knowl.-Based Syst.* **2024**, *296*, 111830. [CrossRef]
6. Wu, Y.; Liang, T.; Gou, J.; Tao, C.; Wang, H. Heterogeneous Mission Planning for Multiple UAV Formations via Metaheuristic Algorithms. *IEEE Trans. Aerosp. Electron. Syst.* **2023**, *59*, 3924–3940. [CrossRef]
7. Chen, J.; Ling, F.; Zhang, Y.; You, T.; Liu, Y.; Du, X. Coverage path planning of heterogeneous unmanned aerial vehicles based on ant colony system. *Swarm Evol. Comput.* **2022**, *69*, 101005. [CrossRef]
8. Yuan, M.; Chen, M.; Zhou, T.; Han, Z. Energy learning hyper-heuristic algorithm for cooperative task assignment of heterogeneous UAVs under complex constraints. *Def. Technol.* **2025**, *54*, 1–14. [CrossRef]
9. Szczerba, R.; Galkowski, P.; Glickstein, I.; Ternullo, N. Robust algorithm for real-time route planning. *IEEE Trans. Aerosp. Electron. Syst.* **2000**, *36*, 869–878. [CrossRef]
10. Ramirez Atencia, C.; Del Ser, J.; Camacho, D. Weighted strategies to guide a multi-objective evolutionary algorithm for multi-UAV mission planning. *Swarm Evol. Comput.* **2019**, *44*, 480–495. [CrossRef]
11. Yao, W.; Qi, N.; Wan, N.; Liu, Y. An iterative strategy for task assignment and path planning of distributed multiple unmanned aerial vehicles. *Aerosp. Sci. Technol.* **2019**, *86*, 455–464. [CrossRef]

12. Yang, P.; Tang, K.; Lozano, J.A.; Cao, X. Path Planning for Single Unmanned Aerial Vehicle by Separately Evolving Waypoints. *IEEE Trans. Robot.* **2015**, *31*, 1130–1146. [CrossRef]
13. Liu, D.; Fei, B.; Bao, W.; Zhu, X.; Li, X. DAWN: Dynamic Task Planning of Multi-UAV With Two-Layer Optimization Mechanism in Uncertain Environments. *IEEE Internet Things J.* **2024**, *11*, 37813–37830. [CrossRef]
14. Dhuheir, M.A.; Baccour, E.; Erbad, A.; Al-Obaidi, S.S.; Hamdi, M. Deep Reinforcement Learning for Trajectory Path Planning and Distributed Inference in Resource-Constrained UAV Swarms. *IEEE Internet Things J.* **2023**, *10*, 8185–8201. [CrossRef]
15. Zhou, Q.; Mao, W.; Nakazato, J.; Ji, Y.; Tsukada, M. Uncertainty-Aware Multi-Agent Reinforcement Learning for Anti-Interference Trajectory Planning of Cellular-Connected UAVs. *IEEE Trans. Veh. Technol.* **2026**, *75*, 2864–2880. [CrossRef]
16. Xu, F.; Zhang, Y.; Wang, R.; Mi, C.; Zhang, Y.; Huang, Y.; Yang, J. Heuristic Path Planning Method for Multistatic UAV-Borne SAR Imaging System. *IEEE J. Sel. Top. Appl. Earth Obs. Remote Sens.* **2021**, *14*, 8522–8536. [CrossRef]
17. Zhou, J.; Zhang, X.; Qin, K.; Yang, F.; Wang, L.; Song, D. Energy-Efficient Target Area Imaging for UAV-SAR-Based ISAC: Beamforming Design and Trajectory Optimization. *Remote Sens.* **2025**, *17*, 2082. [CrossRef]
18. Lu, H.; Yang, Y.; Tao, R.; Chen, Y. Coverage Path Planning for SAR-UAV in Search Area Coverage Tasks Based on Deep Reinforcement Learning. In *2022 IEEE International Conference on Unmanned Systems (ICUS)*; IEEE: New York, NY, USA, 2022; pp. 248–253. [CrossRef]
19. Li, J.; Chen, J.; Wang, P.; Li, C. Sensor-Oriented Path Planning for Multiregion Surveillance with a Single Lightweight UAV SAR. *Sensors* **2018**, *18*. [CrossRef]
20. Li, J.; Xiong, Y.; She, J. UAV Path Planning for Target Coverage Task in Dynamic Environment. *IEEE Internet Things J.* **2023**, *10*, 17734–17745. [CrossRef]
21. Li, J.; Xiong, Y.; She, J.; Wu, M. A Path Planning Method for Sweep Coverage With Multiple UAVs. *IEEE Internet Things J.* **2020**, *7*, 8967–8978. [CrossRef]
22. Galceran, E.; Carreras, M. A survey on coverage path planning for robotics. *Robot. Auton. Syst.* **2013**, *61*, 1258–1276. [CrossRef]
23. Chen, S.; Pei, L.; Gong, J.; Zhou, X.; Li, J.; Wang, C.; Zhao, M.; Li, H.; Cai, Z. Coverage Path Planning of Heterogeneous Unmanned Aerial Vehicles Based on Dual-Stage Genetic Algorithm. In *2024 China Automation Congress (CAC)*; IEEE: New York, NY, USA, 2024; pp. 375–382. [CrossRef]
24. Chen, J.; Du, C.; Zhang, Y.; Han, P.; Wei, W. A Clustering-Based Coverage Path Planning Method for Autonomous Heterogeneous UAVs. *IEEE Trans. Intell. Transp. Syst.* **2022**, *23*, 25546–25556. [CrossRef]
25. Song, J.; Zhao, K.; Liu, Y. Survey on Mission Planning of Multiple Unmanned Aerial Vehicles. *Aerospace* **2023**, *10*, 208. [CrossRef]
26. Dong, X.; Shi, C.; Wen, W.; Zhou, J. Multi-Mission Oriented Joint Optimization of Task Assignment and Flight Path Planning for Heterogeneous UAV Cluster. *Remote Sens.* **2023**, *15*, 5315. [CrossRef]
27. Subash, N.; Nithya, B. UAV Path Optimization Using High-Altitude Data and Mutated Fruit-Fly Strategy. *IEEE Trans. Veh. Technol.* **2025**, *74*, 10151–10161. [CrossRef]
28. Chen, H.X.; Nan, Y.; Yang, Y. Multi-UAV Reconnaissance Task Assignment for Heterogeneous Targets Based on Modified Symbiotic Organisms Search Algorithm. *Sensors* **2019**, *19*, 734. [CrossRef]
29. Tang, J.; Chen, X.; Zhu, X.; Zhu, F. Dynamic Reallocation Model of Multiple Unmanned Aerial Vehicle Tasks in Emergent Adjustment Scenarios. *IEEE Trans. Aerosp. Electron. Syst.* **2023**, *59*, 1139–1155. [CrossRef]
30. Hu, L.; Xi, B.; Yi, G.; Zhao, H.; Zhong, J. A multiple heterogeneous UAVs reconnaissance mission planning and re-planning algorithm. *J. Syst. Eng. Electron.* **2022**, *33*, 1190–1207. [CrossRef]
31. Song, D.; Zhang, X.; Yu, Z.; Qin, K. Coverage Path Planning for Multi-View SAR-UAV Observation System under Energy Constraint. In *IGARSS 2025—2025 IEEE International Geoscience and Remote Sensing Symposium*; IEEE: New York, NY, USA, 2025; pp. 5482–5486. [CrossRef]
32. Mansouri, S.S.; Kanellakis, C.; Georgoulas, G.; Kominiak, D.; Gustafsson, T.; Nikolakopoulos, G. 2D visual area coverage and path planning coupled with camera footprints. *Control Eng. Pract.* **2018**, *75*, 1–16. [CrossRef]
33. Song, R.; Liu, Y.; Bucknall, R. Smoothed A* algorithm for practical unmanned surface vehicle path planning. *Appl. Ocean Res.* **2019**, *83*, 9–20. [CrossRef]
34. Soltani, A.; Tawfik, H.; Goulermas, J.; Fernando, T. Path planning in construction sites: Performance evaluation of the Dijkstra, A*, and GA search algorithms. *Adv. Eng. Inform.* **2002**, *16*, 291–303. [CrossRef]
35. Wu, Y.; Low, K.H.; Lv, C. Cooperative Path Planning for Heterogeneous Unmanned Vehicles in a Search-and-Track Mission Aiming at an Underwater Target. *IEEE Trans. Veh. Technol.* **2020**, *69*, 6782–6787. [CrossRef]
36. Xu, X.; Xie, C.; Ma, L.; Yang, L.; Zhang, T. Multi-objective evolutionary algorithm with two balancing mechanisms for heterogeneous UAV swarm path planning. *Appl. Soft Comput.* **2025**, *173*, 112927. [CrossRef]
37. Karthik, K.; Balasubramanian, C.; Praveen, R. Hybrid golden Jackal and moth flame optimization algorithm based coverage path planning in heterogeneous UAV networks. *Sci. Rep.* **2025**, *15*, 31054. [CrossRef]
38. Zeng, F.; Hu, Z.; Xiao, Z.; Jiang, H.; Zhou, S.; Liu, W.; Liu, D. Resource Allocation and Trajectory Optimization for QoE Provisioning in Energy-Efficient UAV-Enabled Wireless Networks. *IEEE Trans. Veh. Technol.* **2020**, *69*, 7634–7647. [CrossRef]

39. Curlander, J.C.; Mcdonough, R.N. *Synthetic Aperture Radar: Systems and Signal Processing*; Wiley: Hoboken, NJ, USA, 1991.
40. Rodriguez, A.; Laio, A. Clustering by fast search and find of density peaks. *Science* **2014**, *344*, 1492–1496. [CrossRef] [PubMed]
41. Chen, J.; Zhang, Y.; Wu, L.; You, T.; Ning, X. An Adaptive Clustering-Based Algorithm for Automatic Path Planning of Heterogeneous UAVs. *IEEE Trans. Intell. Transp. Syst.* **2022**, *23*, 16842–16853. [CrossRef]
42. Cover, T.; Hart, P. Nearest neighbor pattern classification. *IEEE Trans. Inf. Theory* **1967**, *13*, 21–27. [CrossRef]
43. Fu, Y.; Liu, D.; Chen, J.; He, L. Secretary bird optimization algorithm: A new metaheuristic for solving global optimization problems. *Artif. Intell. Rev.* **2024**, *57*, 123. [CrossRef]
44. Xu, L.; Yuan, C.; Jiang, Z. Multi-Strategy Enhanced Secret Bird Optimization Algorithm for Solving Obstacle Avoidance Path Planning for Mobile Robots. *Mathematics* **2025**, *13*, 717. [CrossRef]
45. Abdel-Basset, M.; Mohamed, R.; Sallam, K.M.; Elsayed, S. Efficient algorithms for optimal path planning of unmanned aerial vehicles in complex three-dimensional environments. *Knowl.-Based Syst.* **2025**, *316*, 113344. [CrossRef]
46. Ma, T.; Wang, T.; Yan, D.; Hu, J. Improved genetic algorithm based on K-Means to solve path planning problem. In *2020 International Conference on Information Science, Parallel And Distributed Systems (ISPDS)*; IEEE: New York, NY, USA, 2020; pp. 283–286. [CrossRef]
47. Bini, E.; Buttazzo, G. Measuring the performance of schedulability tests. *Real-Time Syst.* **2005**, *30*, 129–153. [CrossRef]
48. Du, J.; Huang, B.; Jia, B. An Efficient UAV Coverage Path Planning Method for 3-D Structures. *IEEE Internet Things J.* **2025**, *12*, 31869–31880. [CrossRef]
49. Wei, Z.; Zhu, M.; Zhang, N.; Wang, L.; Zou, Y.; Meng, Z.; Wu, H.; Feng, Z. UAV-Assisted Data Collection for Internet of Things: A Survey. *IEEE Internet Things J.* **2022**, *9*, 15460–15483. [CrossRef]
50. Zhao, Y.; Zheng, Z.; Liu, Y. Survey on computational-intelligence-based UAV path planning. *Knowl.-Based Syst.* **2018**, *158*, 54–64. [CrossRef]

Disclaimer/Publisher's Note: The statements, opinions and data contained in all publications are solely those of the individual author(s) and contributor(s) and not of MDPI and/or the editor(s). MDPI and/or the editor(s) disclaim responsibility for any injury to people or property resulting from any ideas, methods, instructions or products referred to in the content.